LINEAR PREDICTIONS OF SUPERCRITICAL FLOW INSTABILITY IN TWO PARALLEL CHANNELS

By

Maulik Shah

-A- Thesis Submitted to the Faculty of Graduate Studies of
The University of Manitoba
in Partial Fulfillment of the Requirements for the Degree of

MASTER OF SCIENCE

Department of Mechanical and Manufacturing Engineering
University of Manitoba
Winnipeg

THE UNIVERSITY OF MANITOBA

FACULTY OF GRADUATE STUDIES

*****

COPYRIGHT PERMISSION

LINEAR PREDICTIONS OF SUPERCRITICAL FLOW INSTABILITY IN TWO PARALLEL CHANNELS

BY

Maulik Shah

A Thesis/Practicum submitted to the Faculty of Graduate Studies of The University of Manitoba in partial fulfillment of the requirement of the degree

MASTER OF SCIENCE

ABSTRACT

A steady state linear code that can predict thermo-hydraulic instability boundaries in a two parallel channel system under supercritical conditions has been developed. Linear and non-linear solutions of the instability boundary in a two parallel channel system are also compared. The effect of gravity on the instability boundary in a two parallel channel system, by changing the orientation of the system flow from horizontal flow to vertical up-flow and vertical down-flow has been analyzed. Vertical up-flow is found to be more unstable than horizontal flow and vertical down flow is found to be the most unstable configuration. The type of instability present in each flow-orientation of a parallel channel system has been checked and the density wave oscillation type is observed in horizontal flow and vertical up-flow, while the static type of instability is observed in a vertical down-flow for the cases studied here. The parameters affecting the instability boundary, such as the heating power, inlet temperature, inlet and outlet K-factors are varied to assess their effects. This study is important for the design of future Generation IV nuclear reactors in which supercritical light water is proposed as the primary coolant.

ACKNOWLEDGEMENTS

Thanks to my advisor, Dr. V. Chatoorgoon, who offered invaluable guidance, constant encouragement and help at key junctures. Dr. V. Chatoorgoon put faith on my ability and gave me an opportunity to do the wonderful research. Thanks to my examiners, Dr. J. Bartley and Dr. N. Rattanawangcharoen who reviewed my thesis and gave me helpful suggestions. Special thanks to my parents, brother and uncle for their love and moral support during various stages of my life.

DEDICATION

To my loving parents

CONTENTS

LIST OF FIGURES

LIST OF TABLES

NOMENCLATURE

A	Flow area (m^2)
C_K	Friction coefficient in momentum equation (m^{-1})
f	Friction factor
Fr	Froude number
g	Gravitational constant (m/s^2)
G	Mass flux (kg/m^2s)
G_o	Steady state mass flux (kg/m^2s)
h	Enthalpy (kJ/kg)
h_c	Cold side enthalpy (kJ/kg)
h_h	Hot side enthalpy (kJ/kg)
K	K factor
K_1	Channel inlet K-factor or K factor on upstream side of the channel
K_2	Channel outlet K-factor or K factor on downstream side of the channel
L	Length of channel/segments (m)
m	Mass flow rate (kg/s)
m_s	Mass flow rate at the stability boundary (kg/s)
p	Pressure (Pa)
p_{in}	Inlet pressure (Pa)
Δp_{ch}	Channel frictional pressure drop (Pa)
Re	Reynolds's number
Q	Channel power (kW)

Q_s	Power at stability boundary (kW)
s	Laplace transform variable
t	Time period (sec)
T_{cr}	Critical temperature ($^{\circ}C$)
T_{in}	Inlet temperature ($^{\circ}C$)
u	Velocity (m/s)
x	Length of small section (m)

Greek symbols:

Λ	Euler number
ρ	Fluid density (kg/m^3)
ρ_c	Cold side density (kg/m^3)
ρ_h	Hot side density (kg/m^3)
ω	Frequency (sec^{-1})

Subscripts:

0	Steady state
1	For channel 1
2	For channel 2
b	Feed-back
c	Closed loop
ch	Channel
ext	Exit of the channel

f	Feed-forward
in	Inlet to the channel
out	Outlet of the channel
linear	Linear code result
non-linear	Non-linear code result
s	System

Superscripts:

'	Perturbation
$\overline{\quad}$	Average values

CHAPTER 1

INTRODUCTION

Generation IV nuclear reactors are in the research and design stage. The main goals of Generation IV nuclear reactors are to improve nuclear safety, generate electricity at a lower cost, achieve higher thermal efficiency of the plant and improve control of the nuclear processes. Nuclear energy is an attractive alternative to conventional energy sources.

Supercritical light water is proposed as a primary coolant in Generation IV nuclear reactors. Supercritical fluid is the fluid above its critical thermodynamic temperature and pressure. For light water, the critical temperature is 374.3 ^{o}C and the critical pressure is 22.08 MPa. A supercritical fluid behaves like a single-phase fluid and has unique features. It has the unique ability to diffuse through solids like a gas and dissolve materials like a liquid. Another distinctive feature of supercritical fluids is the large change in thermo-physical properties, such as density and specific heat, across the critical point. This large change in density across the critical point can be used effectively to generate a substantial driving head in natural-circulation systems. All these characteristics of supercritical fluids make it an attractive coolant in Generation IV nuclear reactors. By using supercritical water as a coolant, the following advantages may be achieved:

i. Thermal efficiency of the power plant can be improved to 45% as compared to 33% at present. Hence, electricity can be generated at a lower cost.

   (Source: http://en.wikipedia.org/wiki/Supercritical-Water-Cooled_Reactor)

ii. Large changes in density across the critical point provide significant driving head in a natural-convection circulation configuration. Elimination of components such as steam separators and re-circulation pump are possible, which simplify the design and reduce the capital cost.

iii. Plant layout can be simplified.

1.1 OBJECTIVES OF THE WORK

There are certain demerits associated with supercritical light water as a primary coolant (such as material constraints etc.), but one major challenge is thermo-hydraulic instability. Instability generates flow oscillation and possible flow reversal, which is highly undesirable and can cause

i. Overheating of core tubes

ii. Melting of nuclear fuel

iii. Wastage of fuel hence loss of thermal efficiency of plant

iv. Mechanical vibrations

v. Thermal fatigue

The stability of supercritical fluid in parallel channels is a relatively new topic and more research is needed. Supercritical flow in parallel channels is very relevant to the practical situation. The main objectives of the present work are:

- To develop a linear code to predict the thermo-hydraulic instability boundaries for a two parallel channel system.
- To analyze the effect of gravity on the instability boundary by changing the orientation of the system-flow from horizontal to vertical up-flow and vertical down-flow.

- To check the type of instability present in each flow-orientation of a two parallel channel system.
- To assess the effects of various parameters on the instability boundary by changing the parameters such as

i. The heating power applied to the system (50 kW, 100 kW)

ii. The inlet temperature (300 °C, 350 °C)

iii. The channel inlet K-factor (0, 1, 2, 3…)

iv. The channel outlet K-factor (0, 1, 2, 3…)

Here, K factor $= \frac{\Delta p}{\left(\frac{1}{2}\rho u^2\right)}$ where Δp is pressure change across the pressure regulating device in the channel. If the pressure regulating device in the channel is fully open then Δp = 0 and hence, K factor = 0.

1.2 SCOPE OF THE STUDY AND OUTLINE OF THE THESIS

There are two general approaches common for checking the supercritical flow instabilities. They are as follows:

- The linear solution
- The non-linear solution

Linear solutions of supercritical flow in a two parallel channel system are studied here, although some nonlinear solution results are also presented for comparison with the linear solutions. The system pressure was kept constant at 25 MPa (above the critical pressure for water) for all cases. Only the stability of light water is assessed in this work.

To analyze the effect of gravity on the instability boundary in a two parallel channel system, supercritical flow stability has been predicted for three different flow orientations, as shown in Figure 1.1.

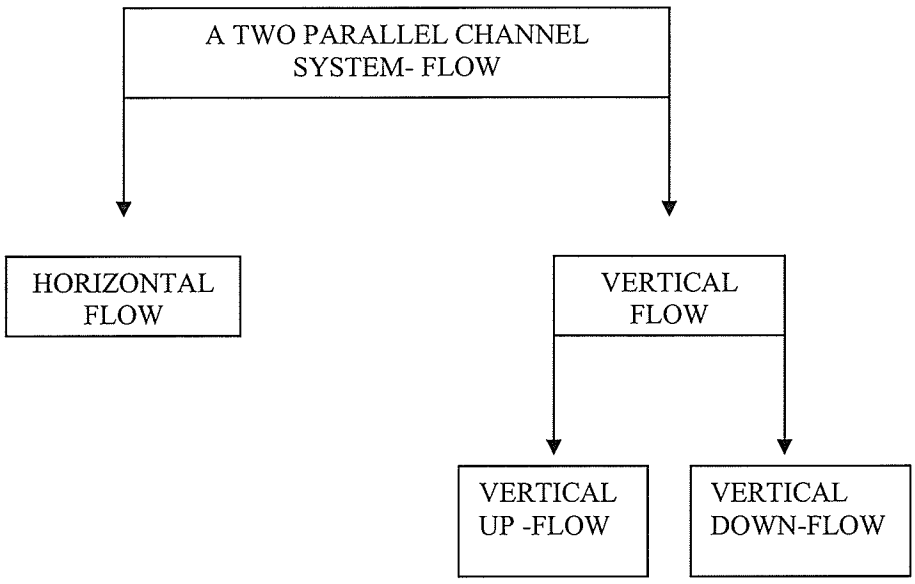

Figure 1.1: Types of system-flow orientation in a two parallel channel system

This thesis contains six chapters including this present chapter-1, Introduction. Chapter -2 covers the literature review on work done by various researchers in the field of supercritical flow stability. Chapter-3 details three different geometries of the system considered in this thesis. Chapter-4 provides the governing equations and boundary conditions for the linear analysis of a two parallel channel system. The linear solution technique for solving the governing equations is also presented. Chapter-5 contains the Results and Discussions for all cases studied. Finally, chapter-6 summarizes the findings and provides recommendations for future work on this topic. The linear code and the

procedure to run the linear code appear in Appendix-A. The complete derivations of the linear governing equations are shown in Appendix-B.

CHAPTER 2

LITERATURE REVIEW

For the design of Generation IV nuclear reactors, flow stability of a system operating in the supercritical region has been a major challenge in the present age. The research carried out by various researchers all over the world for supercritical flow instabilities have been examined in this chapter. Flow instabilities in natural and forced circulation loops, single-phase supercritical and two-phase sub-critical flows and in parallel channels are reported here. More emphasis has been placed on a review of supercritical flow stability in parallel channels. In the following section, a brief introduction on flow instabilities is given. The later sections of the chapter include a literature review on two-phase flow and supercritical flow instabilities.

2.1 FLOW INSTABILITIES

Flow instabilities are usually caused by large momentum changes in the system and strongly depend on the thermodynamic, hydrodynamic and geometric behavior of the system. They may originate as small amplitude oscillations at low power and grow in amplitude with an increase in power, eventually leading to a different operating point or in sustained oscillations.

It was reported in 'Safety Series No. 75-INSAG-7, a report by the International Nuclear Safety Advisory Group' that one of the world's worst nuclear reactor accidents (in the Chernobyl Nuclear Power Plant) occurred on April 25th 1986 in the former USSR. This is as an example of the adverse effects of flow instabilities and the need for a thorough understanding of these instabilities.

According to the region in which the system is operating, instabilities can be categorized as:

i. Single phase sub-cooled instabilities

ii. Two-phase sub-critical instabilities

iii. Single phase supercritical instabilities

2.1.1 SINGLE PHASE SUB-COOLED INSTABILITIES

Single-phase sub-cooled instabilities have been studied in detail for a natural circulation loop configuration by various researchers.

2.1.2 TWO-PHASE SUB-CRITICAL INSTABILITIES

Two-phase flow instabilities can occur whenever fluids in motion are heated or cooled under appropriate flow conditions. Two-phase flow systems can exist in one or more steady states for a given operating condition, and they are prone to flow instabilities. These instabilities usually occur in the form of flow oscillations or flow reversals.

Two-phase flow instability of two-phase flow in parallel channels has been well studied. Such systems often possess multi-valued flow rates for a given channel pressure drop. The two-phase multiplier effect causes a point of inflection in the channel 'pressure-drop (Δp_{ch}) versus flow-rate (m)' characteristic as shown in Figure 2.1. Starting from a high flow rate, with single phase conditions at the outlet, the channel frictional pressure drop decreases with decreasing flow rate; reaches a minimum and then increases with decreasing flow rate due to the two-phase multiplier effect. Flow instability begins to occur at flow rates near the minimum channel frictional pressure drop for horizontal

flow, where $\frac{\partial \Delta p_{ch}}{\partial G} \approx 0$ and the system becomes more unstable as the flow rate decreases further.

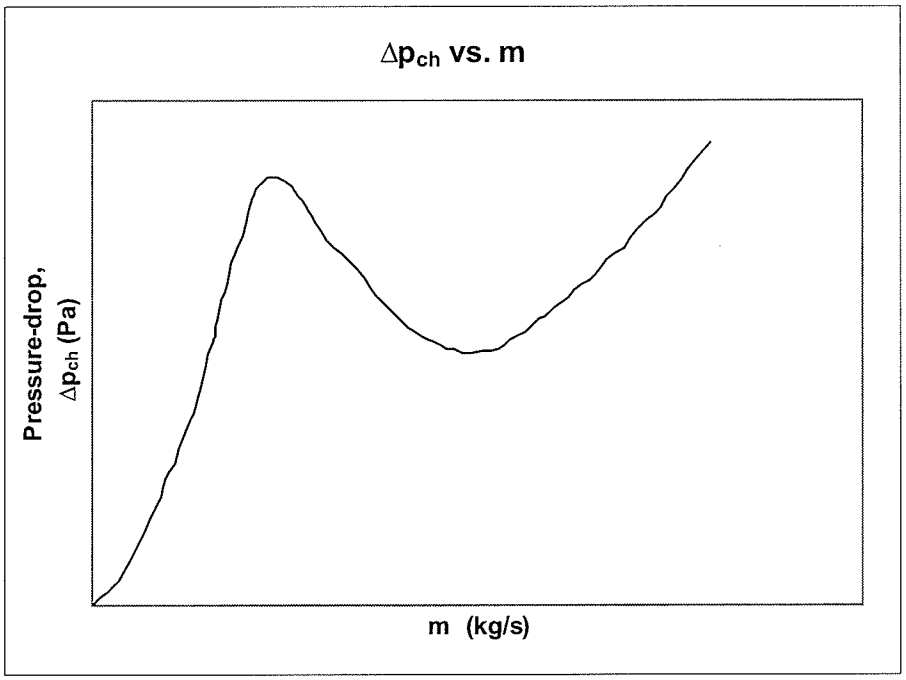

Figure 2.1: 'Pressure-drop vs. flow rate 'in a typical two-phase system (Griffith, 1965)

In general, flow instabilities can be broadly classified into two categories:

i. Static instabilities

ii. Dynamic instabilities

Ledinegg was the first who observed the static type of flow instability. From his name, the static flow instability is also known as ledinegg instability. Static flow instability is characterized by an abrupt large amplitude flow-excursion to a new steady state which may itself be stable or unstable. Therefore, static flow instability is also called an excursive instability. There may be two outcomes of the static instability. One outcome of the static instability may be a different steady state. The other may be just a drifting

away from the initial steady state. A static flow instability can be identified if the system characteristics curve at zero frequency begins at the origin.

A dynamic flow instability is one where the flow, temperature or pressure oscillate. Inertia and other feedback effects play an important role in a dynamic instability. Disturbances are propagated through pressure or density waves. Consequently, the system behaves like a servomechanism and knowledge of the steady state is not sufficient to predict the threshold.

Flow instabilities are further categorized as simple or compound in nature. A simple instability can be explained completely in terms of a single mechanism e.g. Ledinegg or density wave oscillations. An instability is compound in nature when several elementary mechanisms interact in the process, which cannot be studied separately. Table 2.1 details the classification of two-phase flow instabilities, according to Boure et al. (1973).

Table 2.1: Types of instabilities in two-phase flow (Boure et al., 1973)

Class	Type	Cause	Characteristics	Possibility to occur for the present work
1. Static Instabilities				
1.1 Basic static instability	i. Ledinnegg or flow excursion instability	The system attempt to operate in the negative slope region of 'pressure drop versus flow rate' curve	Flow undergoes excursion to a new steady state which may itself be stable or unstable	Known to occur
	ii. Boiling crisis	Ineffective removal of heat from heated surface	Wall temperature excursion and flow oscillation	Not known to occur
1.2 Basic relaxation instability	i. Flow pattern transition instability	Bubbly flow has less void but higher pressure drop than that of annular flow	Cyclic flow pattern transitions and flow rate variations	Not known to occur
1.3 Compound relaxation instability	i. Bumping, geysering, or chugging	Periodic adjustment of meta-stable condition, usually due to lack of nucleation sites	Periodic process of superheat and violent evaporation with possible expulsion and refilling	Not known to occur

2. Dynamic Instabilities				
2.1 Basic (or pure) dynamic instability	i. Acoustic oscillations	Resonance or pressure waves	High frequencies (10-100 Hz) related to time required for pressure wave propagation in system	Known to occur
	ii. Density wave oscillations	Delay and feedback effects in relationship between flow rate, density and pressure drop	Low frequencies (1 Hz) related to transit time of a continuity wave	Known to occur
2.2 Compound dynamic instability	i. Thermal oscillations	Interaction of variable heat transfer coefficient with flow dynamics	Occurs in film boiling	Known to occur
	ii. Boiling water instability	Interaction of void reactivity coupling with flow dynamics and heat transfer	Strong only for small fuel time under low pressures	Not known to occur
	iii. Parallel channel instability	Interaction among small number of parallel channels	Various modes of flow redistribution	Known to occur
2.3 Compound dynamic instability as secondary phenomenon	i. Pressure-drop oscillations	Flow excursion initiates dynamic interaction between channel and compressible volume	Very low frequency periodic process (0.1 Hz)	Known to occur

Among all the types of instabilities tabled above, density wave instabilities have been studied extensively. Density wave type of instability is also called "Flow-void feedback instabilities". It is characterized by low frequency oscillations with an oscillation period approximately one to two times the time required for a fluid particle to travel through the system. Acoustic oscillations are characterized by high frequency oscillation, the period being the same order of magnitude as the time required for a pressure wave to travel through the system. (Boure et al., 1973)

2.1.3 SINGLE PHASE SUPERCRITICAL INSTABILITIES

In supercritical flow there is no known two-phase multiplier effect. Hence, it is inconceivable that $\frac{\partial \Delta p_{ch}}{\partial G} \approx 0$ would apply to a supercritical flow system (Chatoorgoon, 2006). Since supercritical fluids have no definable phase change and the large momentum pressure drops due to the large density change across the critical point could possibly initiate instabilities similar to two-phase flow instabilities. Relatively small amount of work has been done in order to explore the instabilities associated with the supercritical region.

2.2 REVIEW OF TWO-PHASE FLOW INSTABILITIES

Two-phase flow instabilities in parallel channels have been studied extensively, both analytically and experimentally. There are more than four hundred publications on the subject.

Ledinegg (1938) studied flow instability for natural and forced convection in parallel channels systems. Meyer and Rose (1963) theoretically studied parallel-channel instability by developing a momentum integral model. Gambill and Bundy (1964) performed experiments in thin rectangular parallel-channels to study instabilities. Schuster and Berenson (1967) analyzed fire tube forced convection boiler. D'arcy (1968) reported flow instabilities in parallel boiling channels by conducting experiments. Crawley, et al. (1969) studied theoretically two-phase instability in vertical parallel heated channels. Davies and Potter (1969) and Carver (1969) also performed experiments to assess flow instabilities in parallel channels system.

Van Vonderen (1971) carried out both experimental and numerical studies to understand the hydrodynamic behavior of parallel boiling channels. His experiments focused on a parametric study of pressure, inlet sub cooling, and different combinations of channel orifices and the influence of a pump on the stability of parallel channels. He also developed a nonlinear code and simulated the hydrodynamic behavior of three parallel channels using the nonlinear code. Good agreement between theory and experiment was observed. Veziroglu and Lee (1971) did experiments to study boiling flow instabilities in cross-connected parallel channels up-flow systems.

Fukuda and Kobori (1979) were the first to present a perturbation technique to multi channels system. Governing equations for the parallel channel were derived and the

occurrences of instabilities, as well as their modes of oscillations, were derived by solving the characteristic equations. They also classified two-phase flow instabilities into eight different types of instabilities. Of these eight types, three were classified as static instabilities and the other five were classified as dynamic (or density wave) instabilities. Lahey and Drew (1980) also did a detailed review on classification of flow instabilities in two-phase flow.

Podowski et al. (1982) analyzed flow instabilities in condensing channels as contrast to boiling channels. They provided a step-by-step procedure for obtaining the transfer function of the system. They presented results and concluded that, like heated channels, flow instabilities can occur in condensing channels as well. Masanori et al. (1982) studied, analytically and experimentally, density wave instabilities in vertical up-flow parallel boiling channels systems (forced convection). They developed a linear analytical model. They studied the effect of slip ratio on the stability by this linear analytical model and concluded that the difference of the slip ratio on the stability is caused by the difference in the outlet flow conditions, that is, low quality or superheated condition.

Podowski et al. (1986) analyzed two-phase flow instabilities (density wave oscillations) in multi channel systems. D'Auria et al. (1987) developed a linear model for predicting the stability boundary in boiling channels. They used the Nyquist criteria to analyze the stability boundary. Guido et al. (1991) analytically studied density wave oscillation in two identical parallel channels. They used two different approaches for the analysis:

- Perturbation methods

- Fourth order eigen value technique

Duffey and Hughes (1990), Whittle and Forgan (1967), and Duffey, et al. (1993) used the minimum point of the curve of 'Δp versus flow rate' characteristic, as the onset of static instability and derived an analytical expression defining the instability boundary in heated channels.

2.3 REVIEW OF SUPERCRITICAL FLOW INSTABILITIES

Literature on supercritical flow instability is sparse and most of the work is on the heat transfer characteristics. Here, only relevant research work is mentioned.

In 1960, Firstenberg (1960) and Shitzman (1964) reported low frequency flow oscillations in supercritical water, while Griffith (1962) reported low frequency flow oscillations in supercritical R-114. Platt and Wood (1962) also studied low frequency flow oscillations in supercritical oxygen while Ellerbrook, et al. (1962) studied low frequency flow oscillations in supercritical hydrogen. Hines and Wolf (1962) reported low frequency flow oscillations in supercritical RP-1 and DECH.

Walker, et al. (1963) and Harden, et al. (1964) carried out analytical and experimental studies of a natural circulation loop system, with Freon-114 as the working fluid. The exit coolant temperature was near the critical temperature, but did not exceed it. Cornelius, et al. (1965) also reported heat-transfer instabilities (low frequency oscillations) near the critical point. Zuber (1966) was the first one who did an in-depth analysis of the various low frequency instability modes of supercritical fluid flow. He concluded that parameters affecting stabilizing and destabilizing the supercritical flow system are the same as for a two-phase system. He also concluded that supercritical flow instability would be similar to two-phase flow instability, possessing either the excursive or oscillatory types. He derived formulations to support the understanding presented although analytical results were not given.

Jain, et al. (2003) discussed the cause of supercritical flow instability in the Generation IV nuclear power plant. They also discussed the experimental loops existing at the University of Wisconsin, Madison and Argonne National Laboratory (ANL).

Yi, et al. (2004) carried out a linear stability analysis of supercritical-pressure light water (SCLWR-H) at constant supercritical pressure. They also did a parametric study to determine the parameters affecting the stability. Yi, et al. (2004) developed a mathematical model to study the coupled neutronic thermal-hydraulic stability for a high-temperature, supercritical-pressure, light water cooled reactor. Lomperski, et al. (2004) experimentally studied the stability of a natural circulation loop for supercritical carbon dioxide. However, they did not observe any flow oscillations suggested by Chatoorgoon (2001).

Chatoorgoon, et al. (2005) developed non-dimensional parameters, which define the stability boundary in supercritical water in a natural-convection loop. They conducted numerous numerical experiments to propose non-dimensional parameters. These non-dimensional parameters would be useful in facility scaling. They also carried out a similar study using two different fluids, hydrogen and carbon dioxide. Numerical predictions of the flow stability were obtained from the SPORTS code (a non-linear code developed by Chatoorgoon (1986)). Zhao, et al. (2005) presented an approximate three-region model showing the variation of density with enthalpy for sub-critical and supercritical stability analysis. Jain, R., et al. (2006) presented a computational model of both steady state and transient analysis for one dimensional, natural circulation loop of water and CO_2. They proposed dimensionless parameters for generalizing the stability characteristics of the natural-circulation flow loops under supercritical conditions.

Chatoorgoon (2006) reported a non-linear solution for the supercritical flow stability boundary in two horizontal parallel channels and found that the instability boundary lies very close to where $\frac{\partial^2 \Delta p_{ch}}{\partial m^2} = 0$ in the 'Δp_{ch} vs. m' curve, as shown in

Figure 2.2 Here Δp_{ch} is the channel frictional pressure-drop and m is the channel mass flow rate.

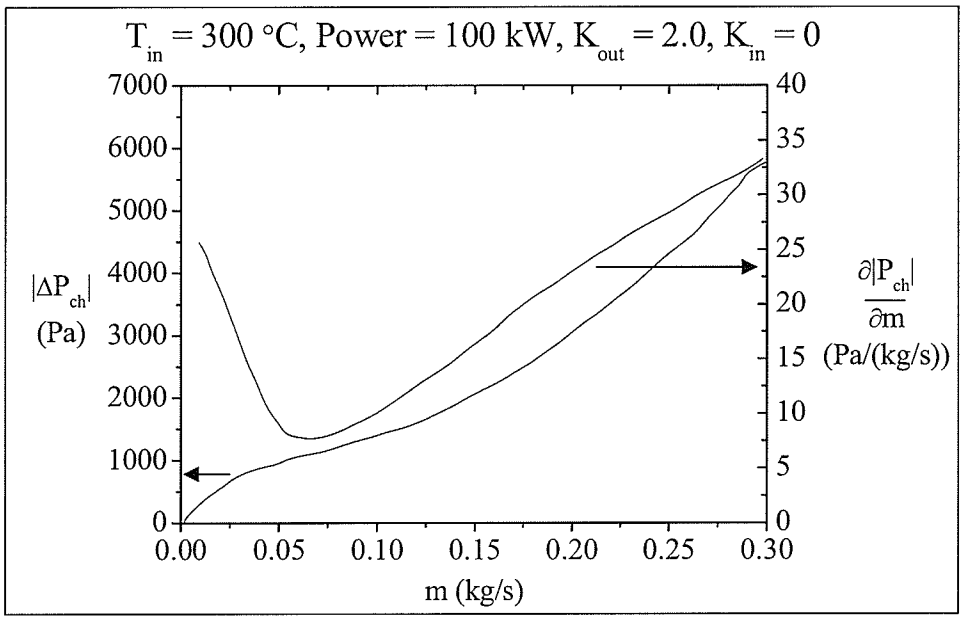

Figure 2.2: 'Channel pressure-drop vs. flow-rate' for supercritical flow in a two horizontal parallel channel system (Chatoorgoon, 2006)

Jain, P., et al. (2006) carried out a linear stability analysis to study supercritical flow instabilities in a natural circulation loop. They obtained stability maps and concluded that the instability behavior of supercritical natural circulation loops was not strictly related to the peak of steady state on the "flow versus power" curve.

Gomez, et al. (2006) carried out both linear and non-linear analysis of the thermo hydraulic stability of a uniformly heated channel at supercritical water conditions. They concluded that in supercritical water systems, static instabilities and pressure-drop oscillations (PDO) will not occur. They used a simplified approximation of the state equation in a bid to keep the analysis simple. Ambrosini, et al. (2006) proposed non-

dimensional parameters for the stability analysis of vertical up-flow in heated channels. The dimensionless parameters for the instability were derived using classical phase change and sub cooling numbers of boiling channels at the pseudo-critical temperature. Contrary to Gomez, et al. (2006), Ambrosini, et al. (2006) found the static instability within the channel using the RELAP code.

Gomez, et al. (2007) studied the influence of the state equation in a linear stability analysis of two identical uniformly heated channels that were coupled by a common inlet and exit plenum. They investigated the neutral stability boundary of two coupled identical channels with a common inlet orifice (Pressure loss coefficient of 3 at the inlet). They concluded that the exact state equation is required to correctly predict the stability boundary. Ambrosini, et al. (2007) assessed the validity of the dimensionless parameters they proposed in Ambrosini, et al. (2006). They showed similarities between supercritical flow stability and two-phase flow stability.

Sharma, et al. (2007) developed a linear code to carry out the analysis of supercritical flow instabilities in a natural circulation loop, and developed stability maps. They concluded that the threshold of the instability is not always equal to the power corresponding to the peak steady state flow and the system can be operated in the negative slope region of the flow-power curve by reducing the feed water inlet temperature. Thus, system efficiency can be improved. Mignot, et al. (2007) discussed the experimental facility that has been built at the University of Wisconsin to study supercritical fluid dynamics during a blow-down or depressurization process through several diameter breaks. They presented preliminary computational analysis, using a standard homogeneous equilibrium model. They implemented a homogeneous

equilibrium model into an Engineering Equation Solver (EES) for predicting results to characterize the depressurization phenomena. They obtained a good agreement between the predicted results from the model with the experimental results. Yang, et al. (2007) proposed a point-hydraulic model to set a criterion for the onset of a sustainable flow oscillation in a closed cooling system. The point-hydraulic model had components such as a heat source, a heat sink, a pump, a pressure control vessel and two throttle valves. They derived the stability maps based on the dimensionless numbers. Based on the stability maps, they discussed the parameters affecting the flow stability of supercritical water-cooled systems. They concluded that the point-hydraulic model gives qualitatively a good agreement with the results from the developed computer code, SASC.

CHAPTER 3

LINEAR SOLUTION

The linear solution method can determine the threshold of instability for infinitesimal perturbations. There are certain advantages associated with the linear solution models over non-linear solution models. They are as follows:

- Linear solution models are much less prone to numerical instabilities.
- Linear solution models are well known for their inherent freedom from temporal and spatial convergence issues.
- Linear solution models yield good engineering solutions with less computational effort and yields results in less time.

However, there are certain disadvantages associated with the linear solution models. They are as follows:

- Linear solution models cannot predict long-term transient unstable behavior.
- Linear solution models do not take non-linear effects of the system into account; therefore, they cannot predict limit-cycle oscillations that are in fact the long oscillatory behavior of the system.
- In general, the predictions of the instability boundary from linear and non-linear solution methods have been comparable and good for two-phase flow. However, there have been reported differences in the prediction of the period of oscillation between the linear and non-linear approaches. There are instances when a system may be unstable by the linear model, but stable by the non-linear model (Gomez, et al. 2006; Lahey, 1992). The exact reason is still unknown.

3.1 GEOMETRY

The configuration of the system must be defined first before proceeding toward the linear solution. In this study, two identical parallel channels were ganged together by common inlet and outlet headers for the prediction of the stability boundary in a two parallel-channel system. The dimensions of the system used were:

- Length of each channel = 3 m
- Heated length of each channel = 2 m
- Length of each upstream/downstream to the heated sections = 0.5 m
- Internal diameter of each channel = 12.7 mm

The same dimensional geometry, which was used for a horizontal flow parallel channel system (Figure 3.1), was used for vertical up-flow and vertical down-flow by changing the orientation of the flow.

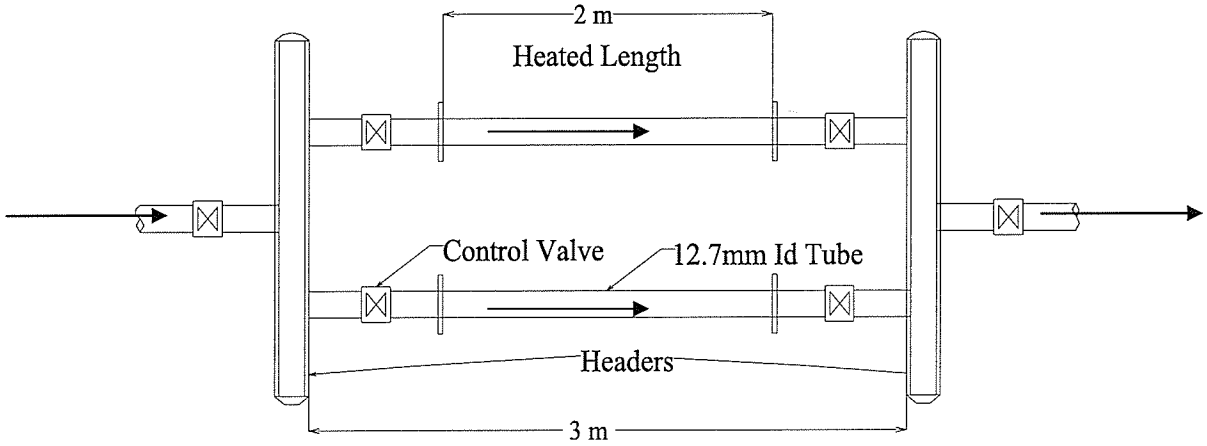

Figure 3.1: Geometry of a horizontal flow- two parallel channel system

In the two-channel geometry considered here, each channel was divided into three segments as shown in Figure 3.2. They are as follows:

i. Upstream to the heated section

ii. Heated section

iii. Downstream to the heated section

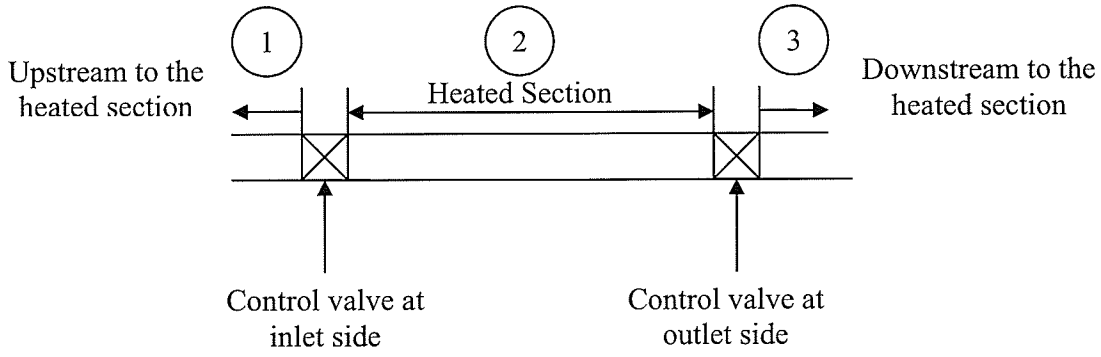

Figure 3.2: Segments of each channel

Each segment was also divided into a number of small nodes for the linear analysis.

The linear solution is presented next. The procedure of the linear solution consists of four steps. They are:

i. Assumptions

ii. Governing equations

iii. Boundary conditions

iv. Linear solution technique

3.2 ASSUMPTIONS

The following assumptions were made in the linear model.

i. One-dimensional flow

ii. Uniform heat flux

iii. Negligible energy stored in the pipe wall

iv. $\rho = f(h)$

v. Negligible effect of the pressure term in the energy equation

3.3 GOVERNING EQUATIONS

The non-linear governing equations for a constant area flow system are (Chatoorgoon et al., 2005):

i. Conservation of Mass (Continuity equation):

$$\frac{\partial \rho}{\partial t} + \frac{\partial (\rho u)}{\partial x} = 0 \ . \tag{3.1}$$

ii. Conservation of Momentum (Momentum transport equation):

$$\frac{\partial (\rho u)}{\partial t} + \frac{\partial (\rho u^2)}{\partial x} + \frac{\partial p}{\partial x} + C_K \rho u^2 + \rho g = 0 \ . \tag{3.2}$$

iii. Conservation of Energy (Energy transport equation):

$$\frac{\partial (\rho h)}{\partial t} + \frac{\partial (\rho u h)}{\partial x} = q_w + \frac{\partial p}{\partial t} \ . \tag{3.3}$$

The term, $\frac{\partial p}{\partial t}$ in the energy equation is usually small in applications as considered here and is omitted for simplicity. Here, q_w is the heat added or removed per flow area per heated length. The above non-linear governing equations were linearized using the small perturbation technique (classical control theory), in Chatoorgoon et al. (2005). The full

derivation of the linearized equations from Equations 3.1, 3.2 and 3.3 is given in Appendix –B. The linearized equations used for the present work are given in the following section.

3.3.1 LINEARIZED EQUATIONS:

Perturbing the conservation of mass equation about the steady state gives

$$\frac{\partial \rho'}{\partial t} + \frac{\partial G'}{\partial x} = 0 . \tag{3.4}$$

Perturbing the conservation of momentum equation about the steady state gives

$$\rho_0 \frac{\partial u'}{\partial t} + G_0 \frac{\partial u'}{\partial x} + G' \frac{du_0}{dx} + \frac{\partial p'}{\partial x} + C_K (G_0 u' + u_0 G') + \rho' g = 0 . \tag{3.5}$$

Perturbing the conservation of energy equation about the steady state gives

$$\rho_0 \frac{\partial h'}{\partial t} + G_0 \frac{\partial h'}{\partial x} + \left(\frac{dh_0}{dx}\right) G' = 0 . \tag{3.6}$$

where, $G = \rho u$.

The linear equations are mapped to a frequency domain using Laplace transformation.

The final form of the linearized equations that were used for predicting the stability boundary:

$$p'_{out} = p'_{in} + s\overline{\left(\nu_1 - \frac{\nu_3}{\gamma_2}\right)}(\rho'_{out} - \rho'_{in}) + \overline{\left(\nu_3 \left(\frac{\gamma_1}{\gamma_2}\right) - \nu_2\right)}(G'_{out} - G'_{in}) . \tag{3.7}$$

where,

$$\rho'_{out} = -\frac{1}{s}\left(\frac{\partial G'}{\partial x}\right)_{out} = -\frac{1}{s}(A_1 \omega_A e^{\omega_A x_s} + B_1 \omega_B e^{\omega_B x_s}) .$$

$$G'_{out} = -\frac{1}{\gamma_2}(A_1 \omega_A e^{\omega_A x_s}(\omega_A + \gamma_1) + B_1 \omega_B e^{\omega_B x_s}(\omega_B + \gamma_1)) .$$

$$\rho_h = \left(\frac{d\rho}{dh}\right)_p .$$

$$s = i\omega .$$

$$A_1 = \frac{(\omega_B G'_{in} + s\rho\rho_{in})}{(\omega_B - \omega_A)} .$$

$$B_1 = \frac{(\omega_B G'_{in} + s\rho\rho_{in})}{(\omega_A - \omega_B)}.$$

$$\omega_A, \omega_B = \frac{-\gamma_1 \pm \sqrt{\gamma_1^2 - 4\gamma_2}}{2}.$$

$$\gamma_1 = [\frac{s}{u_0} - \frac{d(\ln\rho_h)}{dx}].$$

$$\gamma_2 = \frac{-s\rho_h}{G_0}(\frac{dh_0}{dx}).$$

$$\nu_1 = (\frac{u_0^2}{s}).$$

$$\nu_2 = [\frac{1}{s}\frac{d(u_0^2)}{dx} + 2u_0 + C_K(\frac{u_0^2}{s}) - \frac{g}{s}].$$

$$\nu_3 = [s + 2\frac{du_0}{dx} + 2C_K u_0]$$

In the non-heated sections $\frac{dh_0}{dx} = 0.$

Equation 3.7 gives the outlet pressure of each node.

3.4 BOUNDARY CONDITIONS

The following boundary conditions were used for the analysis:

i. $\Delta p'_1 = \Delta p'_2$ (Constant pressure drop for both channels), $p'_{in} = 0$

ii. $G'_{in} = (G'_{in})_1 + (G'_{in})_2 = 0$ or $[(G'_{in})_1 = -(G'_{in})_2]$ (Constant mass flow rate at the inlet of the header)

iii. $T'_{in} = 0$ (Constant inlet temperature)

3.5 LINEAR SOLUTION TECHNIQUE

The values of steady-state properties such as density, velocity, pressure, pressure drop, enthalpy, temperature, C_k, $\left(\frac{\partial\rho}{\partial h}\right)_p$ were obtained from the SPORTS front end, which solves the steady conservation equations to yield the system's steady state solution for each node.

Here, $C_k = \frac{\left(K + \frac{fL}{D}\right)}{2\Delta\Delta} = \frac{\Delta p}{\rho u^2 \Delta x}$ where, f is the friction factor. The formulae used for friction factors for the present study are as follows:

- For turbulent flow: $f = 0.188\,Re^{-0.22}$ (Kondrat'ev (1969)).
- For laminar flow, if it did occur: $f = \frac{64}{Re}$ (which is the same expression for sub-critical, single-phase flow).

The accuracy of these formulae are deemed unimportant for the insights being sought here and these formulae were chosen mainly because they were simple to implement in a one dimensional code, as they do not require both wall and bulk property values. Chatoorgoon (2006) indicated that the $\left(\frac{\partial^2 \rho}{\partial h^2}\right)_p$ term was important to the accurate prediction of the instability boundary in a horizontal supercritical flow parallel channel system.

Knowing the steady-state coefficients of Equation 3.7 from SPORTS, the outlet pressure perturbation of each node can be calculated. The outlet pressure perturbation of one node becomes the pressure perturbation of the next node. Thus, the overall pressure drop perturbation, $\Delta p'$, for each channel can be obtained from Equation 3.7.

3.5.1 THE TRANSFER FUNCTION

To determine the stability of the system, the transfer function of the system needs to be defined first. The transfer function is basically a ratio of the output signal to the input signal. The system stability is examined by applying the tools of control system theory. The feed-forward and feed-back portions of each channel were identified before

the transfer function of each channel was defined. The portion of the channel between the inlet header and the throttle valve on the cold inlet side was defined as the feed-forward part. The rest of the channel was defined as the feed-back part.

Therefore, the feed-forward transfer function for channel 1 is

$$(G_f)_1 = \frac{(G'_{in})_1 u_o}{(\Delta p'_f)_1}, \tag{3.8}$$

where, $(\Delta p'_f)_1$ is the pressure drop perturbation between the inlet and the inlet throttle in channel 1.

The feed-back transfer function for channel 1 is

$$(G_b)_1 = \frac{(\Delta p'_b)_1}{(G'_{in})_1 u_o}, \tag{3.9}$$

where, $(\Delta p'_b)_1$ is the resulting pressure drop perturbation across the entire remaining section downstream of the inlet throttle due to the inlet mass flux perturbation, $(G'_{in})_1$ in channel 1.

According to the rule of transfer functions, the transfer function for channel 1 is

$$(G_c)_1 = \frac{(G_f)_1}{(1+((G_f)_1 (G_b)_1))} = \frac{(G'_{in})_1 u_o}{((\Delta p'_b)_1 + (\Delta p'_f)_1)} = \frac{(G'_{in})_1 u_o}{\Delta p'_1}, \tag{3.10}$$

where $\Delta p'_1 = (\Delta p'_b)_1 + (\Delta p'_f)_1$.

Thus, the characteristic equation of channel 1 is

$$(G_s)_1 = \frac{1}{(G_c)_1} = \frac{\Delta p'_1}{(G'_{in})_1 u_o}. \tag{3.11}$$

Similarly, the characteristic equation of channel 2 is

$$(G_s)_2 = \frac{1}{(G_c)_2} = \frac{\Delta p'_2}{(G'_{in})_2 u_o}. \tag{3.12}$$

The characteristic equation of the overall system of parallel channels becomes

$$G_s = (G_s)_1 + (G_s)_2 = \frac{\Delta p'_1}{(G'_{in})_1 u_o} + \frac{\Delta p'_2}{(G'_{in})_2 u_o} = 0. \quad (3.13)$$

Equation 3.13 is the characteristic equation for a two parallel channel system. The boundary condition 2, $((G'_{in})_1 = -(G'_{in})_2)$ was applied to Equation 3.13 :

$$G_s = \frac{\Delta p'_1}{(G'_{in})_1 u_o} - \frac{\Delta p'_2}{(G'_{in})_1 u_o} = 0. \quad (3.14)$$

$$\frac{\Delta p'_1}{(G'_{in})_1 u_o} = \frac{\Delta p'_2}{(G'_{in})_1 u_o}. \quad (3.15)$$

$$\Delta p'_1 = \Delta p'_2 = \Delta p'_{ch} = 0. \quad (3.16)$$

Equation 3.16 also satisfies the boundary condition 1, $(\Delta p'_1 = \Delta p'_2)$.

3.5.2 THE STABILITY CRITERION

The stability of the system can be determined by the roots of the characteristic equation (Equation 3.13), which are complex numbers. The locus of the all-possible roots of the characteristic equation, for a given frequency sweep, is called the characteristic equation plot of the system. The characteristic equation plot is a graph with the real part of the roots as the abscissa and the imaginary part as the ordinate. The system is said to be stable if the characteristic equation plot crosses the real axis to the right of the origin. The system is said to be unstable if the characteristic equation plot crosses the real axis to the left of the origin. The system is said to be neutrally stable if the characteristic equation plot passes through the origin. The corresponding mass flow rate would define the instability boundary for the given conditions. The frequency of the characteristic

equation plot at the origin would be the frequency of oscillation at the instability boundary (frequency, $\omega = \frac{2\pi}{t}$,where t is the time period).

A sample characteristic equation plot for a vertical up-flow case is shown in Figure 3.3. The characteristic equation plot passes through the origin, which means that it is a stability flow boundary for that particular case.

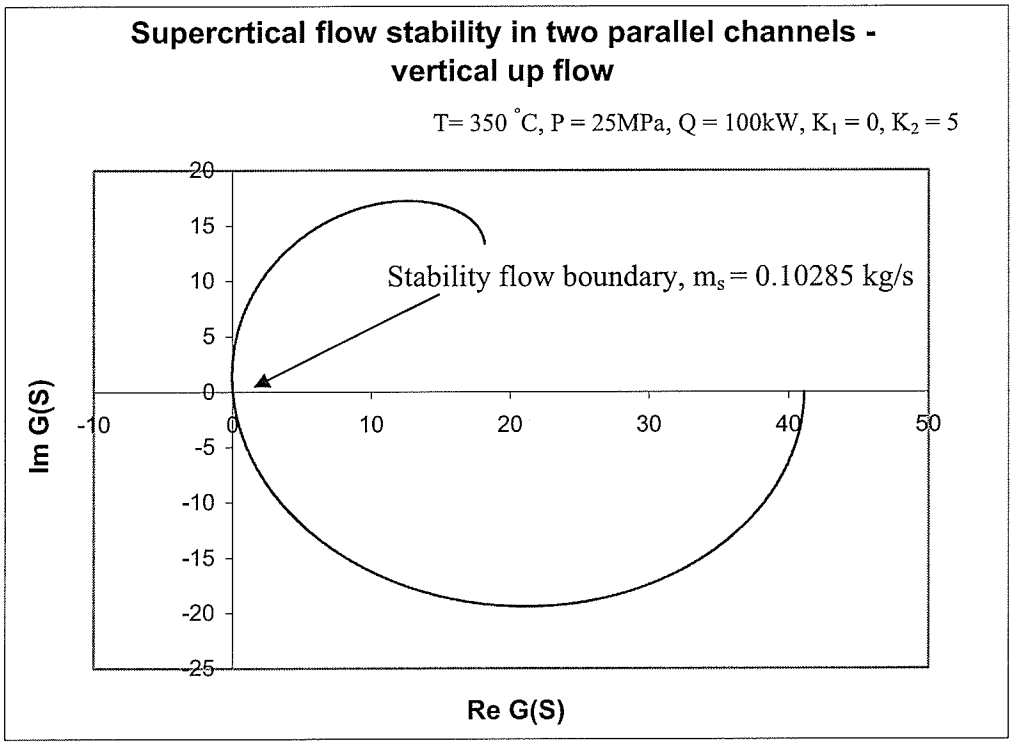

Figure 3.3: The characteristic equation plot -vertical up-flow case

3.5.3 EXTENSION OF PREVIOUS WORK

This research is a continuation of the linear stability analysis of supercritical flow undertaken by Upadhye (2005) in his M.Sc. thesis research. In that work Upadhye

performed a linear stability analysis for supercritical flow in natural-convection loops. Hence, this research begins with the linear code that Upadhye developed.

This is a review and assessment of Upadhye's linear code which was conducted in two ways:

i. A detailed review of the equations and coding of the linear code.

ii. Some of the Upadhye's cases were repeated to verify results.

Major inaccuracies were found in the linear results of Upadhye (2005). The programming errors resulting in inaccurate linear results were identified. The term 'consta', whose value should have been unity, was set to a number other than unity in Upadhye's linear code. This was the main cause for the inaccurate results of Upadhye (2005). The corrected results of some Upadhye's cases are shown in Table 3.1.

Table 3.1: Corrected results for single channel natural circulation loop system-supercritical water cases

T_{in}	K_1	K_2	Height (m)	Heated length (m)	Q_s linear (MW)	Corrected Q_s linear (MW)
350	1	1	13	2	3.95	3.23
350	1	1	10	1	5.30	3.03
330	1	3	13	2	3.05	3.00
330	2	3	13	2	3.15	3.15
330	3	3	13	2	3.30	3.30
330	1	1	13	1	5.15	3.50
330	5	3	13	1	3.80	3.30
360	6	1	13	2	5.65	3.67
360	7	1	13	2	5.80	3.75
360	1	1	13	1	5.90	3.39

3.5.4 THE LINEAR CODE

The linear code that solves the characteristics equation of a two parallel channel system (Equation 3.13) was developed by expanding Upadhye's (2005) linear code for supercritical flow stability in a single channel, natural-circulation loop. The new linear code was used to predict the stability boundary in a two parallel channel system for two different applied powers (50 kW, 100 kW), two different channel inlet flow temperatures (300 $^{\circ}$C, 350 $^{\circ}$C) and different channel inlet and outlet K factors (0, 1, 2, 3, 5...). Several simulations were done for various mass flow rates and the characteristic equation plots were drawn until the stability boundary flow rate was obtained for each case.

This methodology is not applicable to more than two parallel channels and neither is the methodology extendable to more than two parallel channels.

CHAPTER 4

RESULTS AND DISCUSSIONS

This section describes the results for horizontal flow, vertical up-flow and vertical down-flow. The same cases were run for all three orientations and the results were compared. The type of instabilities obtained for each case is noted. The rules that predict the location of the stability boundary for all three system-flow orientations are assessed. Linear and non-linear solutions are also compared.

This chapter is divided into two major parts:

i. Horizontal flow-two parallel channels

ii. Vertical flow-two parallel channels:

   (a) Vertical up-flow

   (b) Vertical down-flow

4.1 HORIZONTAL FLOW -TWO PARALLEL CHANNELS

Non-linear solutions of instability boundaries for horizontal flow parallel channels were generated by Chatoorgoon (2006) using SPORTS code. The linear solutions of the instability boundary are shown in Table 4.1, where $m_{s\text{-non-linear}}$ is the non-linear result of mass flow rate on the instability boundary and $m_{s\text{-linear}}$ is the linear result.

Table 4.1: Comparison of linear and non-linear solutions- horizontal flow

CASE NO:	T_{IN} (°C)	Q (kW)	K_{in}	K_{out}	$m_{s\text{-non-linear}}$ (kg/s)	$m_{s\text{-linear}}$ (kg/s)	% Diff between $m_{s\text{-non-linear}}$ and $m_{s\text{-linear}}$	Time period linear solution (sec)
1	300	50	0	0	0.029	0.031	7.11	19.62
2			0	2	0.036	0.035	-2.77	19.03
3			1	0	0.030	0.030	-0.33	18.47
4			2	0	0.026	0.029	9.31	17.44
5			1	1	0.030	0.032	6.25	18.45
6		100	0	0	0.065	0.063	-3.34	9.92
7			0	2	0.070	0.071	0.88	9.97
8			2	0	0.053	0.057	7.38	8.84
9			1	1	0.064	0.064	0.50	9.37
10	350	50	1	0	0.028	0.031	10.77	9.81
11			0	2	0.035	0.038	8.18	9.66
12			2	0	0.025	0.030	16.19	9.67
13			1.5	1.5	0.034	0.034	1.22	9.51
14			0	10	0.044	0.046	4.16	8.49
15		100	0	0	0.063	0.066	4.96	5.20
16			1	0	0.056	0.063	10.60	5.02
17			0	2	0.073	0.077	5.23	4.87
18			2	0	0.053	0.059	10.68	4.91
19			1.5	1.5	0.066	0.069	4.57	4.79
20			0	5	0.082	0.086	4.52	4.55

- By comparing $m_{s\text{-non-linear}}$ and $m_{s\text{-linear}}$, it is noted that there is close agreement between the non-linear and linear solutions of the stability boundary mass flow rate.

It can also be noted for horizontal flow that

- As the channel inlet K factor increases, while keeping the inlet temperature and power constant, the system becomes more stable. (e.g. compare case number 1, case number 3 and case number 4 in Table 4.1). This is similar to two-phase flow.

- As the channel outlet K factor increases, while keeping the inlet temperature and power constant, the system becomes more unstable. (e.g. compare case number 6 and case number 7 in Table 4.1). This is similar to two-phase flow.
- As the inlet temperature increases, while keeping the power and K factors constant, the system becomes more unstable. (e.g. compare case number 2 and case number 11 in Table 4.1).
- As the applied power increases, while keeping the K factors and inlet temperature constant, the system becomes more unstable. (e.g. compare case number 13 and case number 19 in Table 4.1).

These above stated effects are well known for two-phase flow. Observing the column of time period in Table 4.1, it can be noted that the time period corresponds to the density wave type of instability.

The following parameters were introduced by Chatoorgoon (2006) to explore instability boundaries for horizontal flow in parallel channels: m_b, m_b^*, m_s, m_s^*, where

- m_b is the mass flow rate corresponding to the point where $\frac{\partial^2 \Delta p_{ch}}{\partial m^2} = 0$ in the graph of ' Δp_{ch} vs. m' as shown in Figure 4.1. The value of m_b is obtained from the steady state solution of the system. Here $\Delta p_{ch} = P_{in} - P_{out}$, $P_{in} = p_{in} + \rho_{in} u_{in}^2$ and $P_{out} = p_{out} + \rho_{out} u_{out}^2$.

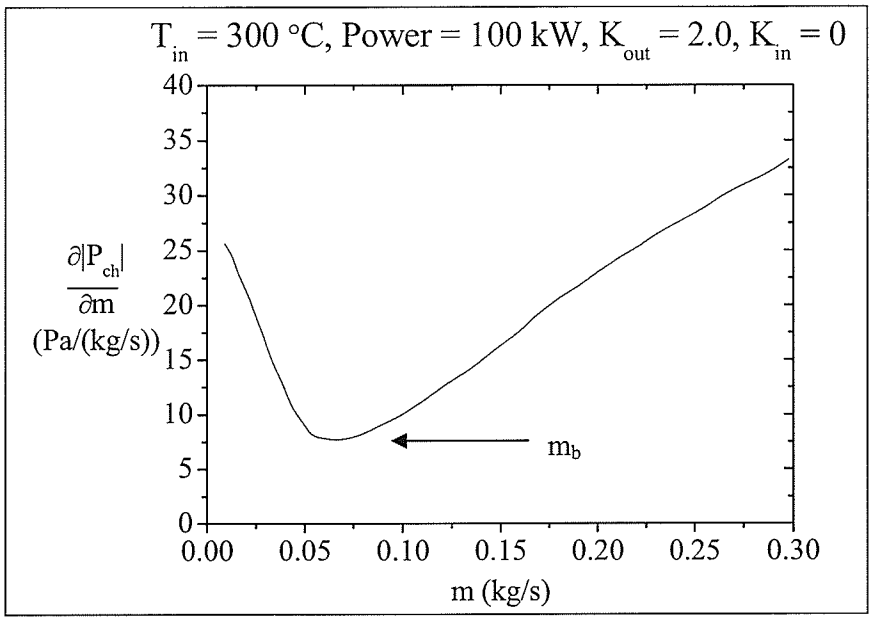

Figure 4.1: Location of stability boundary in horizontal flow
(Chatoorgoon, 2006)

- m_b^* is the non-dimensional mass flow rate corresponding to the point

  where $\frac{\partial^2 \Delta p_{ch}}{\partial m^2} = 0$ in the graph of 'Δp_{ch} vs. m' (Figure 4.1).

  $m_b^* = \frac{m_b h_c}{Q}$, here h_c is the inlet or cold side enthalpy, Q is the channel power.

- m_s is the mass flow rate on the stability boundary in horizontal flow ,which was determined by a stability analysis, either linear or non-linear.

- m_s^* is the non-dimensional mass flow rate at the stability boundary in the horizontal flow:

  $m_s^* = \frac{m_s h_c}{Q}$

Table 4.2: m_b^* and m_s^* obtained from linear and non-linear solutions- horizontal flow

CASE NO:	T_{IN} (°C)	Q (kW)	K_{in}	K_{out}	m_b (kg/s)	m_b^*	m_s^* from non-linear code	m_s^* from linear code
1	300	50	0	0	0.026	0.692	0.772	0.831
2			0	2	0.031	0.825	0.959	0.932
3			1	0	0.024	0.639	0.799	0.796
4			2	0	0.024	0639	0.692	0.763
5			1	1	0.028	0.746	0.799	0.853
6		100	0	0	0.051	0.679	0.865	0.837
7			0	2	0.066	0.879	0.932	0.941
8			2	0	0.048	0.639	0.706	0.762
9			1	1	0.058	0.772	0.852	0.856
10	350	50	1	0	0.027	0.877	0909	1.019
11			0	2	0.035	1.137	1.137	1.238
12			2	0	0.025	0.812	0.812	0.969
13			1.5	1.5	0.032	1.039	1.104	1.118
14			0	10	0.042	1.364	1.429	1.491
15		100	0	0	0.057	0.926	1.023	1.077
16			1	0	0.054	0.877	0.909	1.017
17			0	2	0.071	1.153	1.185	1.251
18			2	0	0.050	0.812	0.861	0.964
19			1.5	1.5	0.064	1.039	1.072	1.123
20			0	5	0.080	1.299	1.332	1.394

Chatoorgoon (2006) determined that the stability mass flow rate boundaries for horizontal flow in parallel channels fall between the lines $m_s^* = m_b^*$ and $m_s^* = m_b^* + 0.2$ in the 'm_s^* vs. m_b^*'plot (Figure 4.2). This indicates that the stability boundary flow rate was either at m_b or slightly above m_b.

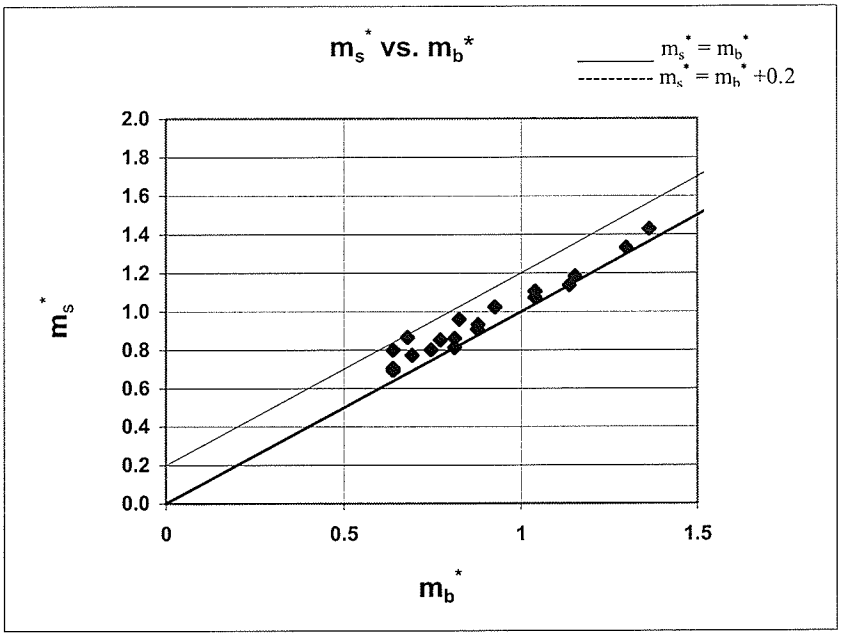

Figure 4.2: Non-linear code results at the instability boundary-horizontal flow (Chatoorgoon, 2006)

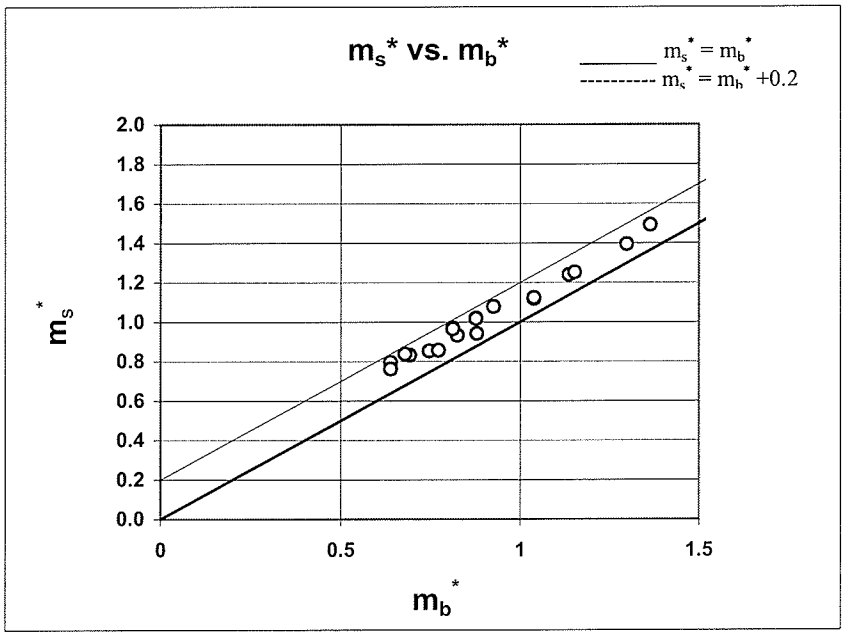

Figure 4.3: Linear code results at the instability boundary-horizontal flow

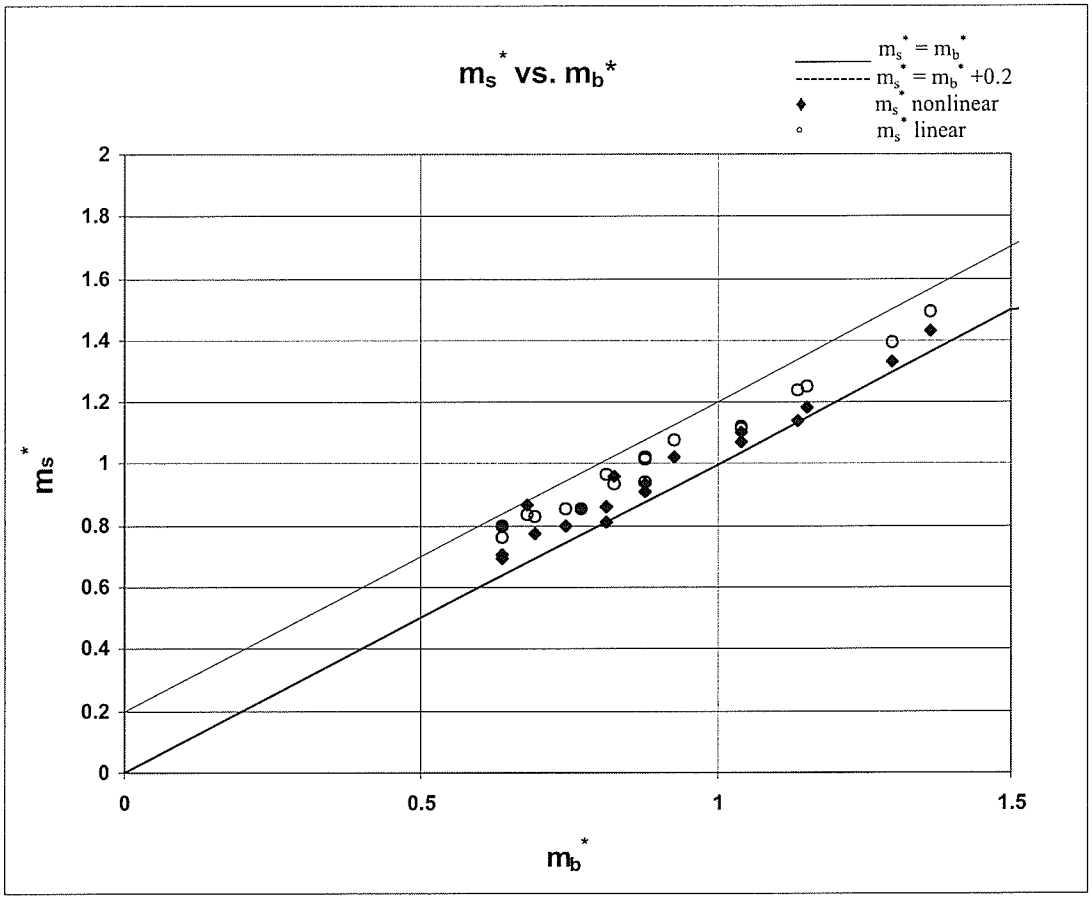

Figure 4.4: Combined non-linear and linear code results at the instability boundary-horizontal flow

In Figure 4.2, m_s^* was obtained from the non-linear code, SPORTS. In Figure 4.3, m_s^* was obtained from the linear code. Figure 4.4 is the combined plot of Figures 4.2 and 4.3. From Figure 4.3, it can be noted that the linear code results also confirm the rule developed by Chatoorgoon (2006). Figure 4.4, which plots the linear and non-linear solutions, shows close agreement between the linear and non-linear solutions of the instability boundary for horizontal flow.

4.2 VERTICAL FLOW- TWO PARALLEL CHANNELS

In this section, vertical up-flow is examined to determine the instability boundary flow rate changes with gravity.

4.2.1 VERTICAL UP-FLOW

The same cases were simulated by changing the orientation of the flow from horizontal flow to vertical up-flow. The results are given in Table 4.3.

Table 4.3: Linear solutions of instability boundary mass flow rate - vertical up-flow

CASE NO:	T_{IN} (°C)	Q (kW)	K_{in}	K_{out}	$m_{s\text{-horizontal}}$ (kg/s)	$m_{s\text{-v-up-flow}}$ (kg/s)	Time period (sec)
1	300	50	0	0	0.031	0.086	4.75
2			0	2	0.035	0.080	4.90
3			1	0	0.030	0.082	4.80
4			2	0	0.029	0.079	4.83
5			1	1	0.032	0.079	4.87
6		100	0	0	0.063	0.124	3.42
7			0	2	0.070	0.111	3.39
8			2	0	0.057	0.107	3.45
9			1	1	0.064	0.110	3.51
10	350	50	1	0	0.031	0.078	3.71
11			0	2	0.038	0.075	3.88
12			2	0	0.030	0.072	3.76
13			1.5	1.5	0.034	0.070	3.85
14			0	10	0.046	0.062	4.36
15		100	0	0	0.066	0.111	2.67
16			1	0	0.063	0.101	2.68
17			0	2	0.077	0.105	2.77
18			2	0	0.059	0.093	2.71
19			1.5	1.5	0.069	0.095	2.79
20			0	5	0.086	0.103	2.92

- By comparing the column of stability mass flow boundary in horizontal flow, $m_{s\text{-horizontal}}$ and the column of stability mass flow boundary in vertical up-flow, $m_{s\text{-v-up-flow}}$, it can be noted that vertical flow is more unstable than horizontal flow. In all cases $m_{s\text{-v-up-flow}}$ is greater than $m_{s\text{-horizontal}}$.

It can be also noted for vertical up-flow from Table 4.3 that

- As the channel inlet K factor increases, while keeping the inlet temperature and power of the system constant, the system becomes more stable. (e.g. compare case number 1, case number 3 and case number 4 in Table 4.3). This effect is similar to the horizontal flow case.
- As the channel outlet K factor increases, while keeping the inlet temperature and power constant, the system becomes more stable. (e.g. compare case number 6 and case number 7 in Table 4.3). This result is opposite to the horizontal flow case. The same increment of the channel inlet K factor yields a more stable system than the channel outlet K factor (e.g. compare case number 15, case number 17 and case number 18 in Table 4.3).
- As the inlet channel flow temperature increases, while keeping the power and K factors constant, the system becomes more stable. This effect was opposite to the horizontal flow case (e.g. compare case number 2 and case number 11 in Table 4.3).
- As the applied power increases, while keeping the inlet temperature and K factors constant, the system becomes more unstable (e.g. compare case number 13 and case number 19 in Table 4.3). This result is similar to the horizontal flow case.

By observing the column of time period in Table 4.3, it is noted from the time period that the oscillation is of the density wave type. A simple rule for determining the location of the stability boundary in vertical up-flow is still unknown at this moment. The work presented in this thesis is new to the field of supercritical flow instabilities.

4.2.1.1 COMPARISON WITH THE WORK OF AMBROSINI ET AL. (2006)

This section reports on a case reported in the literature by Ambrosini, et al. (2006) and duplicated here with the linear code developed. Ambrosini, et al. studied vertical up-flow in a single heated channel in which the flowing fluid was at supercritical pressure, as shown in Figure 4.5. They applied a constant pressure-drop boundary condition to their system. They proposed dimensionless parameters based on an analogy of two-phase flow and presented results obtained from the world-renowned RELAP code.

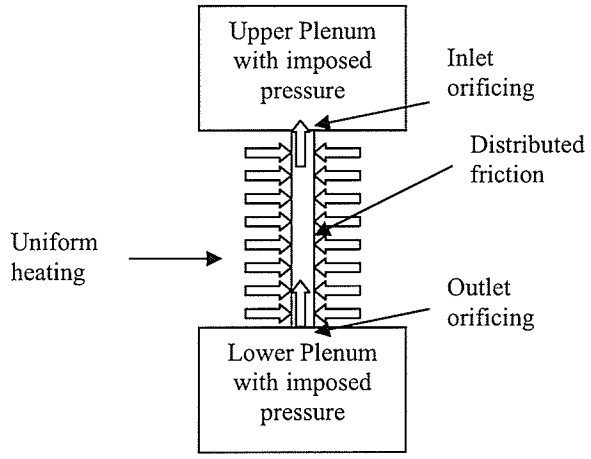

Figure 4.5: Heated channel model of Ambrosini et al. (2006)

It is fruitful to compare Ambrosini et al. (2006) work with the present work to verify our own code results. Therefore, one case, which was given in Figure 18 of Ambrosini et al. (2006), was re-run with the linear code of this thesis. The case details are:

- 48 nodes
- Friction dimensionless group (Euler number), $\Lambda = 22$
- Froude number, $Fr = 0.046$
- $K_{in} = 10.5$

- $K_{out} = 3$
- Channel length = 4.2672 m
- Hydraulic diameter =3.4 mm
- Courant Number = 0
- Coolant flow area = $5.49*10^{-5}$ m^2
- System pressure = 25 MPa
- Inlet temperature = 280 $^{\circ}C$
- Linear power = 25 kW/m

For the above case, Ambrosini et al. (2006) reported the stability boundary mass flow rate was 0.11 kg/s. Our linear result of the stability boundary mass flow-rate is 0.102 kg/s, while the non-linear code (SPORTS) result is 0.10 kg/s.

Thus, a good agreement was achieved between the results of the RELAP code and the linear code used in this thesis, which verifies the linear code results. This also leads to another important finding, which is the analysis of a single heated channel system is sufficient to predict the stability boundary mass flow rate for any number of channels. Even though the boundary conditions of Ambrosini et al. (2006) are different than the present work, the result was almost the same. Therefore, it can be said that a constant pressure drop boundary condition is also applicable to parallel channels.

4.2.1.1 EFFECT OF HIGHER K FACTORS

At higher K factors, however, some interesting findings for the stability mass flow rate in vertical up-flow are noted (Table 4.4).

Table 4.4: Effect of large K factors -vertical up-flow

T_{IN} (°C)	Q (kW)	K_{in}	K_{out}	$m_{s\text{-horizontal}}$ from linear code (kg/s)	$m_{s\text{-linear}}$ (kg/s) for vertical-up flow	$m_{s\text{-non-linear}}$ (kg/s) for vertical-up flow
300	50	3	3	0.035	0.046	nf
		5	5	0.037	0.040	nf
	100	3	3	0.066	0.091	0.072
		5	5	0.069	0.083	0.070
350	50	3	3	0.037	0.052	nf
		5	5	0.039	0.045	nf
	100	3	3	0.071	0.087	0.073
		5	5	0.073	0.082	0.070
		10	10	0.075	0.075	-

nf – not found

It can be noted from Table 4.4 that for vertical up-flow at higher K factors,

- The results of linear code and non-linear code do not agree for K factors of 3 or greater in vertical up-flow. The exact reason is unknown at this time.
- At higher K factors, the stability boundary for vertical up-flow approaches the stability boundary of horizontal flow. In other words, the frictional pressure drop dominates over the gravity. Above K factors (approximately 3 for the non-linear solution) the instability boundary becomes the same for horizontal and vertical up-flows and gravity does not have any effect on the stability boundary.

- The non-linear code SPORTS, didn't predict any instability boundary for cases where the power = 50kW and the system was vertical. SPORTS found the system to be always stable. The reason is unknown at this time.

4.2.2 VERTICAL DOWN-FLOW

In this section, the results of vertical down-flow are discussed. The results are given in Table 4.5.

Table 4.5: Linear solutions of instability boundary mass flow rate - vertical down-flow

CASE NO:	T_{IN} (°C)	Q (kW)	K_{in}	K_{out}	$m_{s\text{-}v\text{-}up\text{-}flow}$ (kg/s)	$m_{s\text{-}v\text{-}down\text{-}flow}$ (kg/s)
1	300	50	0	0	0.086	0.153
2			0	2	0.080	0.136
3			1	0	0.082	0.145
4			2	0	0.079	0.137
5			1	1	0.079	0.137
6		100	0	0	0.124	0.211
7			0	2	0.111	0.187
8			2	0	0.107	0.187
9			1	1	0.110	0.183
10	350	50	1	0	0.078	0.152
11			0	2	0.075	0.143
12			2	0	0.072	0.144
13			1.5	1.5	0.070	0.137
14			0	10	0.062	0.107
15		100	0	0	0.111	0.209
16			1	0	0.101	0.191
17			0	2	0.105	0.176
18			2	0	0.093	0.177
19			1.5	1.5	0.095	0.164
20			0	5	0.103	0.141

- By comparing the column of stability mass flow boundary in vertical up-flow, $m_{s\text{-}v\text{-}up\text{-}flow,}$ and the column of stability mass flow boundary in vertical down-flow, $m_{s\text{-}v\text{-}down\text{-}flow,}$ it is noticed that vertical down-flow is more unstable than vertical up-flow. The flow rate at the instability boundary is much higher in down-flow than in up-flow.

It is also noticed that

- As the channel inlet K factor increases, while keeping the inlet temperature and power constant, the system becomes more stable (e.g. compare case number 1, case number 3 and case number 4). This effect is similar to the horizontal flow case.
- As the channel outlet K factor increases, while keeping the inlet temperature and power constant, the system becomes more stable. (e.g. compare case number 6 and case number 7). This effect is opposite to the horizontal flow case.

  The same increment of the channel inlet K factor yields a more stable system than the channel outlet K factor (e.g. compare case number 15, case number 17 and case number 18 in Table 4.5).
- As the inlet temperature increases, while keeping the power and K factors constant, the system becomes more unstable. This is opposite to the vertical up-flow cases (e.g. compare case number 2 and case number 11 in Table 4.5), but is similar to the horizontal flow case.
- As the applied power increases, keeping the inlet temperature and K factors constant, the system becomes unstable. This is similar to the vertical up-flow and horizontal flow cases (e.g. compare case number 13 and case number 19 in Table 4.5). So it can be concluded that gravity doesn't affect the trend due to power increase.

By observing the stability curves for all the vertical down-flow cases, it is noted that the stability plot starts from the origin at zero frequency. This indicates a static instability. Hence it is a static instability and not a density wave oscillation in vertical down-flow.

One such case of static instability is shown in Figure 4.6, where the plot starts from the origin.

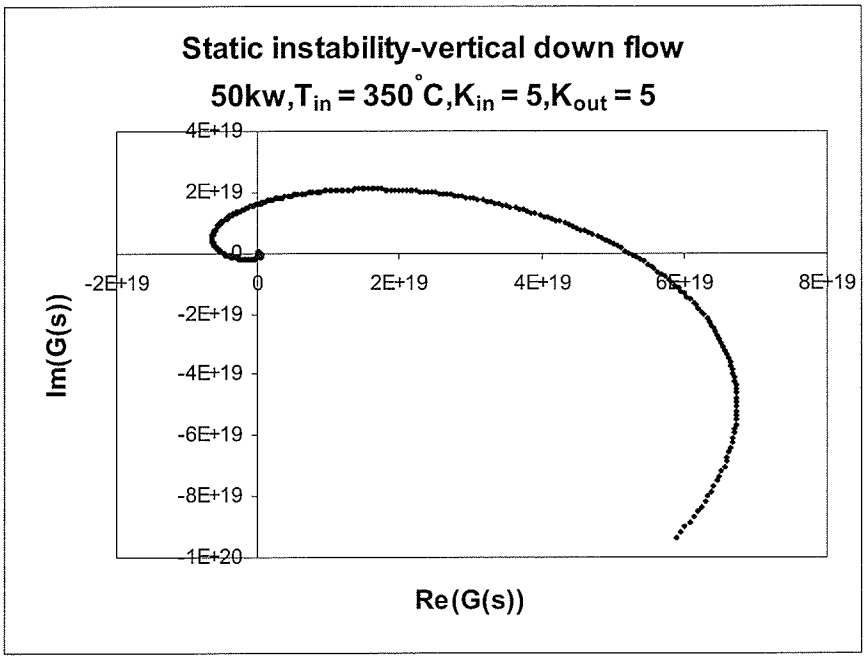

Figure 4.6: Static instability in vertical down-flow

The rule that determines the location of the stability boundary in vertical down-flow was uncovered by Chatoorgoon (personal communication). The rule states that the stability boundary in vertical down-flow lies near the lowest point on the graph '(P_{in}-P_{out}) vs. m'. The following parameters were introduced by Chatoorgoon (personal communication) to explore the instability boundaries for vertical down-flow.

- m_d is the mass flow rate corresponding to the point where $\frac{\partial(P_{in}-P_{out})}{\partial m}=0$ in the graph of '(P_{in}-P_{out}) vs. m' as shown in Figure 4.6. The value of m_d is obtained from the steady state solution of the system.

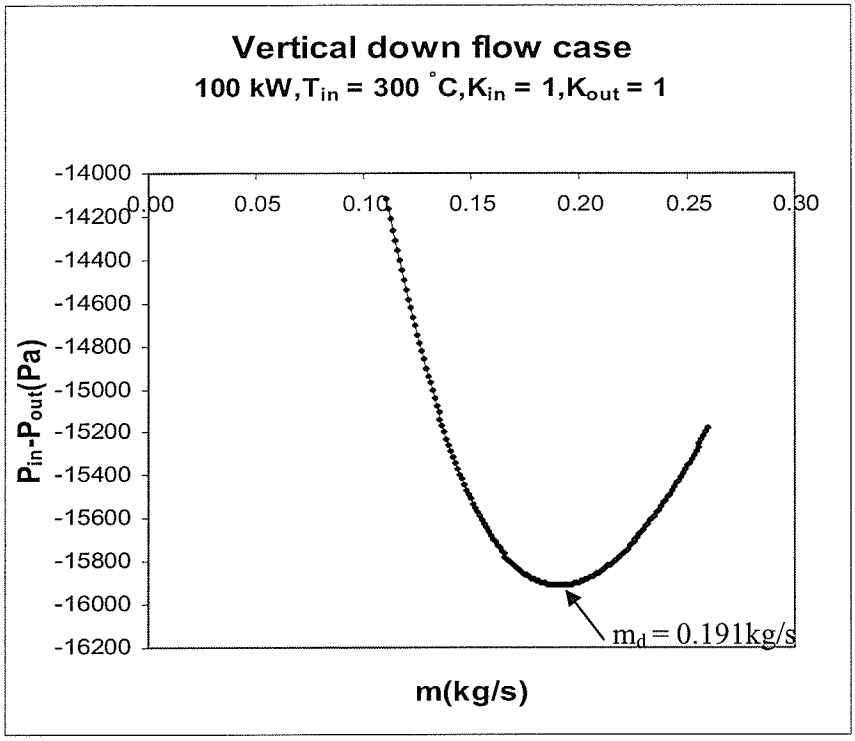

Figure 4.7: Location of stability boundary in vertical down-flow

- m_d^* is the non-dimensional mass flow rate corresponding to the point where $\frac{\partial(P_{in} - P_{out})}{\partial m} = 0$ in the graph '$(P_{in}$-$P_{out})$ vs. m':

$$m_d^* = \frac{m_d h_c}{Q}$$

- $m_{s\text{-}v\text{-}down\text{-}flow}$ or m_s is the mass flow rate on the stability boundary in vertical down-flow determined by the linear stability code.
- m_s^* is the non-dimensional mass flow rate at the stability boundary in vertical down-flow determined by the linear stability code:

$$m_s^* = \frac{m_s h_c}{Q}$$

Table 4.6 compares m_d with $m_{s\text{-}v\text{-}down\text{-}flow}$. The differences are minor, indicating very good agreement. Thus, it can be concluded that the stability boundary mass flow in vertical down-flow lies either at m_d or slightly below m_d.

Table 4.6: Comparison of instability boundary mass flow rate, $m_{s\text{-}v\text{-}down\text{-}flow}$ with m_d - vertical down-flow

CASE NO:	T_{IN} (°C)	Q (kW)	K_{in}	K_{out}	$m_{s\text{-}v\text{-}down\text{-}flow}$ (kg/s)	m_d	% Difference between $m_{s\text{-}v\text{-}down\text{-}flow}$ and m_d	m_s^*	m_d^*
1	300	50	0	0	0.153	0.157	2.61	4.073	4.180
2			0	2	0.136	0.141	3.68	3.621	3.754
3			1	0	0.145	0.149	2.76	3.860	3.967
4			2	0	0.137	0.141	2.92	3.648	3.754
5			1	1	0.137	0.141	2.92	3.648	3.754
6		100	0	0	0.211	0.213	0.95	2.809	2.836
7			0	2	0.187	0.189	1.07	2.489	2.516
8			2	0	0.187	0.189	1.07	2.489	2.516
9			1	1	0.183	0.191	4.37	2.436	2.543
10	350	50	1	0	0.152	0.159	4.61	4.937	5.164
11			0	2	0.143	0.148	3.50	4.644	4.807
12			2	0	0.144	0.149	3.47	4.677	4.839
13			1.5	1.5	0.137	0.141	2.92	4.449	4.579
14			0	10	0.107	0.110	2.80	3.475	3.572
15		100	0	0	0.209	0.215	2.87	3.394	3.491
16			1	0	0.191	0.201	5.24	3.102	3.264
17			0	2	0.176	0.176	0.00	2.858	2.858
18			2	0	0.177	0.182	2.82	2.874	2.955
19			1.5	1.5	0.164	0.167	1.83	2.663	2.712
20			0	5	0.141	0.148	4.96	2.290	2.403

All instability data fall between the line $m_s^* = m_d^*$ and the line $m_s^* = m_d^* - 0.2$, indicating the stability boundary mass flow rate, m_s is always slightly less than m_d (Figure 4.7).

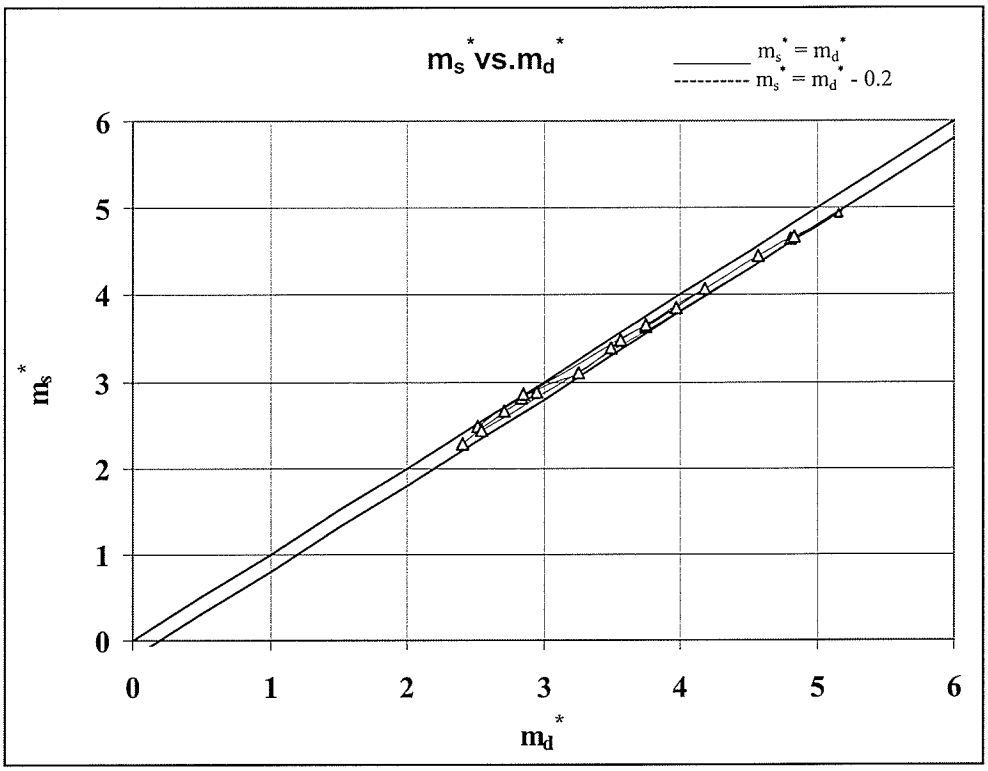

Figure 4.7: Linear code results at the instability boundary - vertical down-flow

4.3 SPATIAL CONVERGENCE

To ensure spatial convergence in the linear code, small node lengths (~2 cm) were assigned in the heated section of each channel and 10 cm node lengths were used outside the heated section of each channel for the linear analysis. Small node lengths were used due to the large density change across each node and the derivative term, $\left(\frac{\partial \rho}{\partial h}\right)_p$, which does not exist in the non-linear code, but which exists in the linear code. A fine mesh was required to accurately capture its effect.

To verify the spatial convergence of the results of predicted flow rate at the stability boundary obtained with 2 cm node lengths, a few cases were run using 1 cm node lengths. The results of predicted flow rate at the instability boundary obtained with the 1 cm node lengths were essentially the same as those obtained with 2 cm node lengths. Upadhye (2005) used both 10 cm section lengths and 5 cm section lengths in his linear model and found similar agreement. Thus, the results presented in this chapter are regarded as satisfactorily converged solutions of the instability boundary.

4.4 TEMPORAL CONVERGENCE

The non-linear code (SPORTS) did not require as small node lengths. Node lengths of 10 cm generally gave good results. However, 2 cm segments were used to be consistent with that used in the linear model. The non-linear code did require small time steps. The time step of 0.05 second was used to generate temporally converged solutions. Because the SPORTS code was formulated with a fully implicit finite-difference scheme, it does not have a large time-step limitation. In fact, it converges even for an infinite time step. However, to achieve temporal convergence for the flow instability simulations, the time step and node lengths must be judiciously chosen.

CHAPTER 5

CONCLUSIONS AND RECOMMENDATIONS

Linear predictions of the supercritical flow stability boundary in a two parallel channel system were studied. The effect of gravity was also studied including up-flow and down-flow. The type of instability occurring in each system was determined. The effects of various parameters on the instability boundary were assessed.

5.1 CONCLUSIONS

Based on the cases studied, the following conclusions can be made:

a) Vertical flow is more unstable than horizontal flow.

b) Vertical down-flow is more unstable than vertical up-flow. The instability boundary flow-rate for vertical up-flow lies between the cases of horizontal flow and vertical down-flow cases.

c) It is confirmed that in horizontal flow, the stability boundary lies very close to where $\frac{\partial^2 \Delta p_{ch}}{\partial m^2} = 0$, as discovered and reported by Chatoorgoon (2006).

d) The threshold of the stability flow boundary in vertical down-flow occurs very close to where $\frac{\partial (P_{in} - P_{out})}{\partial m} = 0$ as discovered and reported by Chatoorgoon (Personal communication).

e) In horizontal flow, an increase in the inlet K factor enhances system stability while an increase in the outlet K factor diminishes system stability. In vertical-flow (either up or down), an increase in the inlet K factor enhances system

stability, while an increase in the outlet K factor also slightly enhances system stability.

f) In horizontal flow, an increase in the flow inlet temperature destabilizes the system. This is also true for vertical down-flow. However, the trend is reversed for vertical up-flow.

g) Irrespective of the orientation of the system, an increase in the channel power yields a more unstable system.

h) There is good agreement on the flow-rate at the instability boundary between the linear and non-linear solutions, except at higher K factors in vertical up-flow.

i) In vertical up-flow, the results of linear code and non-linear code do not agree for the K factors greater than 3. The reasons are unknown at this time.

j) The non-linear solution of vertical up-flow approaches the horizontal flow solution when the K factors in the inlet and outlet sides are high (≥ 3 in non-linear code, ≥ 10 in the linear code). Above these K factors, the instability mass flow boundary becomes the same for horizontal and vertical up- flow and the gravity doesn't play any role on the instability mass flow rate boundary.

k) Density wave oscillation occurred in horizontal flow and vertical up-flow for the cases studied here. Static instability only occurred in all the vertical down-flow cases. (Ambrosini and Chatoorgoon found occurrence of static instability in horizontal flow and vertical up-flow at low inlet temperatures)

l) Analysis of a single heated channel system with constant pressure drop boundary conditions is sufficient to predict the stability boundary mass flow rate for any number of channels.

5.2 RECOMMENDATIONS

- Experiments are needed to verify these results. The supercritical flow facility at the University of Manitoba has been constructed and is ready to conduct instability tests for testing these findings.
- More study is recommended to explain the differences between the non-linear code and linear code results for vertical flow at higher K factors.
- More study is recommended for vertical up-flow.
- More work is recommended to study the effects of wall heat and a pump on the stability boundary.

REEFERENCES

[1] http://en.wikipedia.org/wiki/Supercritical-Water-Cooled_Reactor.

[2] Ambrosini, W., Di Marco, P., Ferreri, J.C., 2000. 'Linear and Nonlinear Analysis of Density-wave Instability Phenomenon', Heat and Technology, Calore, Technologia, Vol.18, n.1.

[3] Ambrosini, W., Sharabi, M., 2006. 'Dimensionless Parameters in Stability Analysis of Heated Channels with Fluids at Supercritical Pressures', Proceedings of ICONE14, International Conference on Nuclear Engineering, Miami, Florida.

[4] Ambrosini, W., Sharabi, M., 2007. 'Assessment of Stability Maps for Heated Channels with Supercritical Fluids versus the Predictions of a System Code', 3rd International Symposium on SCWR-Design and Technology, Shanghai, China.

[5] Boure, A., Bergles, A.E., Tong, 1973. 'Review of Two-Phase Flow Instability', Nuclear Engineering and Design, 25, pp.165-192.

[6] Carver, M.B., 1969. 'Effect of By-pass Characteristics on Parallel-Channel Flow Instabilities', Proc. Instn. Engrs, 18, Pt 3C, paper 11.

[7] Carver, M.B., Chatoorgoon, V., Stewart, D.G., 1985. 'Validation of the DYML Boiling Instability Program', BNES 3rd Int. Conf. in Boiler Dynamics, Harrogate, UK.

[8] Chatoorgoon, V., 1986. 'SPORTS-A Simple Thermal hydraulic Stability Code', Nucl. Eng. Design 93, p. 51-67.

[9] Chatoorgoon, V., 2001. 'Stability of Supercritical Fluid Flow in a Single-Channel Natural-Convection Loop', International Journal of Heat and Mass Transfer, 44, pp.1963-1972.

[10] Chatoorgoon, V., Voodi, A., Fraser, D., 2005. 'The Stability Boundary for Supercritical Flow in Natural Convection Loops, Part I: H2O Studies', Nucl. Eng. and Design 235, pp. 2570-2580.

[11] Chatoorgoon, V., Voodi, A., Upadhye, P., 2005. 'The Stability Boundary for Supercritical Flow in Natural Convection Loops, Part II: CO2 and H2 Studies', Nucl. Eng. and Design 235, pp. 2581-2593.

[12] Chatoorgoon, V., Upadhye, P., 2005. 'Analytical Studies of Supercritical Flow Instability in Natural-Convection Loops', 11th International Topical Meeting on Nuclear Reactor Thermal-Hydraulics (NURETH-11), Oct 2-6, Avignon, France.

[13] Chatoorgoon, V., 2006. 'Supercritical Flow Stability in Two Parallel Channels', Proceedings of Int. Conf. of Nuclear Engineering, ICONE 14-89692, July 17-20, Miami, Florida.

[14] Chatoorgoon, V. Shah, M., Duffey, R., 2007. 'Linear predictions of supercritical flow instability in parallel channels', 3rd Int. Symposium on SCWR Design and Technology, – March 12-15, Shanghai, China.

[15] Cornelius, A. J., Parker, J. D., 1965. Heat Transfer Instabilities Near the Critical Point, Proceedings of the 1965 Heat Transfer and Fluid Mechanics Institute, Stanford University Press, pp. 317-329.

[16] Crawley, J.D., Gouse, S.W., Deane, C., 1969. 'Two-Phase Flow Oscillations in Vertical, Parallel, Heated Channels', Proc. of the Symposium on Two-Phase Flow Dynamics, EURATOM, 2, p. 1132- 71.

[17] D'arcy, D. F., 1968. 'An Experimental Investigation of Boling Channel Flow Instability,' AECL-2733.

[18] Dashkiyev, Y. G., Rozhalin, V. P., 1975. 'Thermo-Hydraulic Stability of a System of Steam-Generating Channels with Super-Critical Pressure', Heat Transfer, Soviet Research, Vol.7, No. 5.

[19] D'Auria, F., Sanctis, N. D., Marco, P.D., Lahey, R. T., Podowski, M. Z., 1987. 'A Linear Model to Study Fluid dynamic Instabilities in Boiling Channels due to Density Oscillations,' Heat and Technology, 5(3-4), pp.55-72.

[20] Davies, A.L., Potter, R., 1969. 'An Analysis of the Cause of Unstable Flow in Parallel Channels', Proc. of the Symposium on Two-Phase Flow Dynamics, EURATOM, 2, pp. 1225-1266.

[21] Dimmick, G. R., Spinks, N. J., Duffey, R. B., 1998. 'An Advanced CANDU Reactor with Supercritical Water Coolant: Conceptual Design Features', 6th International Conference on Nuclear Engineering, San-Diego, California, 10-14.

[22] Dimmick, G. R., Chatoorgoon, V., Khartabil, H. F., Duffey, R.B., 2002. 'Natural-Convection studies for advanced CANDU reactor concepts', Nucl. Eng. and Design 215, 27-38.

[23] Duffey, R.B., Hughes, E.D., 1990. 'Static Flow Instability Onset in Tubes, Channels, Annuli and Rod Bundles', Proc. ASME, Heat Transfer Division, 150, Thermal Hydraulics of Advanced Nuclear Reactors, pp. 145-159.

[24] Duffey, R.B., Hughes, E.D., 1991. 'Static Flow Instability Onset in Tubes, Channels, Annuli and Rod Bundles', Int. Journal of Heat Mass Transfer, 34 (10) pp. 2483-2496.

[25] Duffey, R.B., Hughes, E.D., Rohatgi, U.S., 1993. 'Two-Phase Flow Stability and Dryout in Parallel Channels in Natural Circulation', National Heat-Transfer Conference, Atlanta, GA, AIChE Symposium Series, 89, pp. 44-50.

[26] Ellerbrook, H.H., Livingood, J.N., Straight, D.W., 1962. NASASP- 20, pp. 27.

[27] Firstenberg, H., Goldmann, K., Hudson, J.H., 1960. 'Boiling Songs and Associated Mechanical Vibrations', NDA-2131-12. Heat Transfer and Fluid Mechanics Institute, Stanford University Press, pp. 317-329.

[28] Fukuda, K., Hasegawa, S., 1979. 'Analysis on Two Phase flow instability in parallel multi channels', J.Nucl.Sci. Tech. 16, 190-191.

[29] Gambill, W.R., Bundy, R.D., 1964. 'Heat Transfer Studies of Water Flow in Thin Rectangular Channels, Parts I & II', Nucl. Sci. Engng. 18, pp. 69-89.

[30] Gomez, T. Ortega, Class, A., Lahey, R .T, Schulenberg, T., 2007. 'Stability Analysis of Heated Flow channels with Supercritical Water', 3rd International Symposium on SCWR-Design and Technology.

[31] Gomez, T. Ortega, Class, A., Lahey, Jr., R.T., Schulenburg, T., 2006. 'Stability Analysis of a Uniformly Heated Channel with Supercritical Water', Proceedings of Int. Conf. of Nuclear Engineering, ICONE 14-89733, Miami, Florida.

[32] Griffith, J.D., 1962. 'Geysering in Liquid-Filled Lines', ASME, paper no. 62-HT-39.

[33] Griffith, 1965. 'Notes on Pressure drop-flow rate instabilities in two phase system'.

[34] Guido, G., Converti, J., and Clausse, A., 1991. 'Density-wave Oscillation in Parallel Channels-An Analytical Approach', Nuclear Engineering Design 125-136.

[35] Harden, D.G., Boggs, J. H., 1964. 'Transient Flow Characteristics of a Natural-Circulation Loop Operated in the Critical Region', Proceedings of the 1964 Heat Transfer and Fluid Mechanics Institute, Stanford University Press, pp. 38-50.

[36] Hines, W.S., Wolf, H., 1962. 'Pressure Oscillations Associated with Heat Transfer to Hydrocarbon Fluids at Supercritical Pressures and Temperatures', ARS Journal, 32, pp. 361-366.

[37] Jain, P., Rizwan-Uddin, 2006. 'Steady-State and Dynamic Analyses of Supercritical CO_2 Natural Circulation Loop', Proceedings of Int. Conf. of Nuclear Engineering, ICONE 14-89103, Miami, Florida.

[38] Jain, R., J. Litch, M. Anderson, M. Corradini, S. Lomperski and D. H. Chao, 2003. 'Studies of Natural Circulation Heat Transfer and Flow Stability of a Supercritical Fluid', The 10^{th} International Topical Meeting on Nuclear Reactor Thermal Hydraulics (NURETH-10), Seoul, Korea.

[39] Jain, R., Corrandini, M.L, 2006. 'A Linear Stability Analysis for Natural-Circulation Loops under Supercritical Conditions', Nuclear Technology.

[40] Kondrat'ev, N.S., 1969. 'Heat Transfer and Hydraulic Resistance with supercritical water flowing in tubes', Thermal Engineering, 16 (8), pp. 73-77.

[41] Ledinegg, M., 1938. 'Instability of Flow during Natural and Forced Convection', Die Warme, 61 (8), pp. 891-8.

[42] Lomperski, S., Cho, D. H, Jain, R., Corradini, M. L., 2004.'Stability of a Natural Circulation Loop with a Fluid Heated Through the Thermodynamic Pseudo critical Point,' Proceedings of International Congress on Advances in Nuclear Power Plants, Pittsburgh, USA, pp.1736-1741.

[43] Masanori, A., shigebumi, A., Akira, I., 1982. 'Instabilities in Parallel Channel of Forced-Convection Boiling Up flow System, (V)' Research Laboratory for Nuclear Reactors, Tokyo Institute of Technology.

[44] Meyer, J.E., Rose, R.P., 1963. 'Application of a Momentum Integral Model to the Study of Parallel Channel Boiling Flow Oscillations', J. of Heat Transfer, Trans. ASME series C, 85.

[45] Mignot, G., Anderson, M., Corradini, M., 2007. 'Critical Flow Experiment and Analysis for Supercritical Fluid', 3rd International Symposium on SCWR-Design and Technology, Shanghai, China.

[46] Platt, C.K., Wood, C.C., 1962. Adv in Cryogenic Engr., 7, pp. 296, Plenum Press.

[47] Podowski, M., Lahey, R. T., 1982. 'Density-Wave Oscillations', Proceedings of 9th U.S. National Congress of Applied Mechanics, Cornell University, pp.101-107.

[48] Podowski, M., Taleyarkhan, R.P., Lahey, Jr., R.T., 1986. 'Channel to channel instabilities in Parallel boiling systems'.

[49] Schuster, J.R., Berenson, P.J., 1967. 'Flow Stability of a Five-Tube Forced Convection Boiler', American Society of Mechanical Engineers, paper 67-WA/HT-20.

[50] Sharma, M., Bagul, R. K., Pilkhwal, D.S., Vijayan, P.K., Saha, D., Sinha, R.K., 2007. 'Linear Stability Analysis of a Supercritical Water Natural Circulation Loop', 3rd International Symposium on SCWR-Design and Technology, Shanghai, China.

[51] Shitzman, M.E., 1964. Paper # 1-59, 2nd Al-Union Conf. on Heat and Mass Transfer, Minsk.

[52] Upadhye, P., 2005, 'Stability Studies of Supercritical Flow in Single Channel Natural Circulation Loop'. M.Sc. Thesis, University of Manitoba, Canada.

[53] Van Vonderen, A.C.N., 1971. 'On the Hydrodynamic Behavior of Parallel Boiling Water Channels,' Ph.D. Thesis, Eindhoven University of Technology, Netherlands.

[54] Veziroglu, T.N., Lee, S.S., 1971. 'Boiling-Flow Instabilities in a Cross-Connected Parallel-Channel Up-flow System', ASME 71-HT- 12.

[55] Whittle R.H., Forgan, R., 1967. 'A correlation for the minima in the pressure drop versus flow-rate curves for sub-cooled water flowing in narrow heated channels', Nucl. Eng. & Des., 6, pp. 89-99.

[56] Walker, B. J., 1964. 'The 'Density Effect' Model: Prediction and Verification of the Flow Oscillation Threshold in a Natural- Circulation Loop Operating Near the Critical Point', ASME Paper No. 64-WA/HT-23.

[57] Yang, Y.H, Cheng, X., 2007. 'A Point-Hydraulic Model for Flow Stability Analysis', 3rd International Symposium on SCWR-Design and Technology, Shanghai, China.

[58] Yi, T. T., Koshizuka, S., Oka, Y., 2004. 'A Linear Stability Analysis of Supercritical Water Reactors', (II) Coupled Neutronic Thermal-Hydraulic Stability, Journal of Nuclear Science and Technology, 41, No.12, pp.1176-1186

[59] Yi, T. T., Koshizuka, S., Oka, Y., 2004. 'A Linear Stability Analysis of Supercritical Water Reactors', (I) Thermal-Hydraulic Stability, Journal of Nuclear Science and Technology, 41, No.12, pp.1166-1175.

[60] Zhao, J., Saha, P., Kazimi, M., 2005. 'Stability of Supercritical Water-Cooled Reactor During Steady-State And Sliding Pressure Start-Up', 11th International

Topical Meeting on Nuclear Reactor Thermal-Hydraulics (NURETH-11), Avignon, France.

[61] Zuber, N., 1966. 'An Analysis of Thermally induced Flow Oscillations in the Near-Critical and Super-Critical Thermodynamic Region', Rept. NASA-CR-80609, Research and Development Center, general Electric Company, Schenectady, New York, USA.

APPENDIX-A

A.1 LINEAR CODE - TWO PARALLEL CHANNELS

```
fprintf ('This is a linear code to predict the supercritical flow stability boundary in a two parallel channel system" prepared by Maulik Shah\n');
MER=xlsread('C:\Documents and Settings\umshah2\Desktop\350-50-3-3(1).xls');% Excel file for channel-1 be saved and read. Use SPORTS code for SS solution
KER=xlsread('C:\Documents and Settings\umshah2\Desktop\350-50-3-3(2).xls');%Excel file for channel-2 be saved and read. Use SPORTS code for SS solution
fprintf('Assigning the values to variables starts now\n');
% some important quantities are defined first for channel-1 & channel-2.
inhnd=6;% number of nodes from inlet to inlet header.1
chinnd=7;% This is  first number of node to inlet for both channels 1&2.
chextnd=157;% This is  last number of node up to exit  .
fprintf('Total number of nodes are \n');
totalnd=164%

%Column 0ne: Node Number. Just for recognition, not used actually in the code.

%the data input to the code is done now from excel file for channel 1
for k=1:totalnd
   delx(k,1)=MER(k,2);      % Column 2: The node length will be same for both channel 1&2.
   Uo(k,1)=MER(k,3);        % column 3: SS Velocity at each node.
   velgrad(k,1)=MER(k,4);  % column 4: d(uo)/dx,for each node.
```

```
ho(k,1)=MER(k,5);       % column 5: SS enthalpy for each node.
hograd(k,1)=MER(k,6);   % column 6: d(h0)/dx for each node.
Go(k,1)=MER(k,7);       % column 7: mass flux for each node.
const1(k,1)=MER(k,8);   % column 8: d(rho)/dh 0r d(density)/dh using NIST package.
fricfact(k,1)=MER(k,9); % column 9: this is friction factor
gravity(k,1)=MER(k,10); % column 10: gravity factor of each node.
var0(k,1)=MER(k,11);    % column 11: u0^2.
delUosq(k,1)=MER(k,12); % column 12: this is d(u0^2)/dx or d(u0*u0)/dx.
var1(k,1)=MER(k,13);    % column 13: 1/[d(rho)/dh].
var2(k,1)=MER(k,14);    % column 14:d{[1/[d(rho)/dh]]}/dx.
        const2(k,1)=MER(k,15);  % column 15: This is product of column 8*column14.

end
                                                        % Upadhye (2005)
%the data input to the code is done now from excel file for channel 2
for k=1:totalnd
   Uo2(k,1)=KER(k,3);       % column 3: SS Velocity at each node.
   velgrad2(k,1)=KER(k,4);  % column 4: d(uo)/dx,for each node.
   ho2(k,1)=KER(k,5);       % column 5: SS enthalpy for each node.
   hograd2(k,1)=KER(k,6);   % column 6: d(h0)/dx for each node.
   Go2(k,1)=KER(k,7);       % column 7: mass flux for each node.
   const12(k,1)=KER(k,8);       % column 8: d(rho)/dh 0r d(density)/dh using NIST
package.
```

```
   fricfact2(k,1)=KER(k,9); % column 9: this is friction factor
   gravity2(k,1)=KER(k,10); % column 10: gravity factor of each node.
   var02(k,1)=KER(k,11);    % column 11: u0^2.
   delUosq2(k,1)=KER(k,12); % column 12: this is d(u0^2)/dx or d(u0*u0)/dx.
   var12(k,1)=KER(k,13);    % column 13: 1/[d(rho)/dh].
   var22(k,1)=KER(k,14);    % column 14:d{[1/[d(rho)/dh]]}/dx.
   const22(k,1)=KER(k,15);  % column 15: This is product of column 8*column14

end
                                                        % Upadhye (2005)

fprintf('Reading of files are completed\n');

totlth = 0.0;%length of the system

for k=1:totalnd
   totlth = totlth+delx(k,1);
end
fprintf('Total length of system is \n');
totlth

% Code will start running from this point.
consta=1;
```

```
w=0.1:0.025:2.5;% frequency
% Defining the Imaginary Number,
i=sqrt(-1);
s=i*w;

gper=1; % Density on cold side (G') at the start of first node ,gper is (gprime).
gdper=0.0;%Value of gdper d(gprime)/dx at start of first node is defined,gdper is
(gdprime).


gper1in=1*gper; %mass flow rate at inlet header or inlet of the channel-1
gper1=gper1in;
gdper1=gdper;
ppertotch1=0;%presurre perturbation of the channel-1
gper2in=-gper1in;%mass flow rate at inlet header or inlet of the channel-2 -Boundary
condition
gper2=gper2in;
gdper2=gdper;

ppertotch2=ppertotch1;%presurre perturbation of the channel-2-Boundary condition

for k=chinnd:chextnd
```

```
x1=0.0;
x2=(x1+delx(k,1));
if hograd(k,1)==0
eta1=((s./Uo(k,1))+(const2(k,1)));
C=0;
c1=((C)./(eta1));
eta2=0; % Since d(ho)/dx is equal to ZERO for 'Non-Heated Sections'
A=gper1-(c1.*x1) +((gdper1-c1)./(eta1)); % equations were coded from here.
B=((c1- gdper1)./((eta1).*(exp(-eta1.*x1))));
gper1=(A+((B).*(exp((-eta1).*x2)))+(c1.*(x2)));
gdper1=(((B).*(-eta1).*(exp(-eta1.*x2)))+c1);
ppera1=(s+2*fricfact(k,1)*Uo(k,1)+2*velgrad(k,1)).*((A.*((x2)-(x1)))+((B.*((exp(-
eta1.*x2))-(exp(-eta1.*x1)))./(-eta1))+(0.5*(c1).*((x2*x2)-(x1*x1))));
pperb1=(((delUosq(k,1))./s)+2*(Uo(k,1))+((fricfact(k,1)*(Uo(k,1)^2))./s)-
((gravity(k,1))./s)).*((B.*((exp(-eta1.*x2))-(exp(-eta1.*x1))))+(c1).*(x2-x1));
pperc1=(((Uo(k,1).^2)./s).*(B.*(-eta1).*((exp(-eta1.*x2))-(exp(-eta1.*x1)))));
else
eta1=((s./Uo(k,1))+(const2(k,1)));
eta2=(-((s./Go(k,1)).*const1(k,1)).*consta.*hograd(k,1));
root1=((-eta1)+(sqrt(((eta1).^2)-4*eta2)))./2;
root2=((-eta1)-(sqrt(((eta1).^2)-4*eta2)))./2;
CP=0;
A=((root2).*gper1-gdper1-((CP).*(root2)))./((root2-root1).*(exp(root1.*x1)));
```

```
B=((root1).*gper1-gdper1-((CP).*(root1))./((root1-root2).*(exp(root2.*x1)));
gper1=(A.*(exp(root1.*x2))+(B.*(exp(root2.*x2)))+CP);
gdper1=(A.*(root1).*(exp(root1.*x2))+(B.*(root2).*(exp(root2.*x2))));
ppera1=(s+2*fricfact(k,1)*Uo(k,1)+2*velgrad(k,1)).*(((A.*(((exp(root1.*x2))-
(exp(root1.*x1))))./(root1))+((B.*(exp(root2.*x2)-exp(root2.*x1))./(root2))+(CP.*(x2-
x1)));
pperb1=(((delUosq(k,1))./s)+2*(Uo(k,1))+(((fricfact(k,1))*(Uo(k,1)^2))./s)-
((gravity(k,1))./s)).*((A.*((exp(root1.*x2))-(exp(root1.*x1))))+(B.*((exp(root2.*x2))-
(exp(root2.*x1)))));
pperc1=(((Uo(k,1)^2)./s).*((A.*(root1).*((exp(root1.*x2))-
(exp(root1.*x1))))+(B.*(root2).*((exp(root2.*x2))-(exp(root2.*x1))))));
 end
  ppertotch1=ppertotch1+ppera1+pperb1+pperc1;

end
                                                        % Upadhye (2005)
ppertotch1;%presurre perturbation at outlet or exit of the channel-1
 for k=chinnd:chextnd
     x1=0.0;
     x2=(x1+delx(k,1));
  if hograd2(k,1)==0
     eta1=((s./Uo2(k,1))+(const22(k,1)));
     C=0;
```

```
c1=((C)./(eta1));
eta2=0; % Since d(ho)/dx is equal to ZERO for 'Non-Heated Sections'
A=gper2-(c1.*x1) +((gdper2-c1)./(eta1));
B=((c1- gdper2)./((eta1).*(exp(-eta1.*x1))));
gper2=(A+((B).*(exp((-eta1).*x2)))+(c1.*(x2)));
gdper2=(((B).*(-eta1).*(exp(-eta1.*x2)))+c1);
ppera2=(s+2*fricfact2(k,1)*Uo2(k,1)+2*velgrad2(k,1)).*((A.*((x2)-
(x1)))+((B.*((exp(-eta1.*x2))-(exp(-eta1.*x1)))./(-eta1))+(0.5*(c1).*((x2*x2)-
(x1*x1))));
pperb2=(((delUosq2(k,1))./s)+2*(Uo2(k,1))+((fricfact2(k,1)*(Uo2(k,1)^2))./s)-
((gravity2(k,1))./s)).*((B.*((exp(-eta1.*x2))-(exp(-eta1.*x1))))+(c1).*(x2-x1));
pperc2=(((Uo2(k,1).^2)./s).*(B.*(-eta1).*((exp(-eta1.*x2))-(exp(-eta1.*x1)))));

else

eta1=((s./Uo2(k,1))+(const22(k,1)));
eta2=(-((s./Go2(k,1)).*const12(k,1)).*consta.*hograd2(k,1));
root1=((-eta1)+(sqrt(((eta1).^2)-4*eta2)))./2;
root2=((-eta1)-(sqrt(((eta1).^2)-4*eta2)))./2;
CP=0;
A=((root2).*gper2-gdper2-((CP).*(root2)))./((root2-root1).*(exp(root1.*x1)));
B=((root1).*gper2-gdper2-((CP).*(root1)))./((root1-root2).*(exp(root2.*x1)));
gper2=(A.*(exp(root1.*x2))+(B.*(exp(root2.*x2)))+CP);
```

```
gdper2=(A.*(root1).*(exp(root1.*x2))+(B.*(root2).*(exp(root2.*x2))));
ppera2=(s+2*fricfact2(k,1)*Uo2(k,1)+2*velgrad2(k,1)).*(((A.*(((exp(root1.*x2))-
(exp(root1.*x1))))))./(root1))+((B.*(exp(root2.*x2)-exp(root2.*x1))))./(root2))+(CP.*(x2-
x1)));
pperb2=(((delUosq2(k,1))./s)+2*(Uo2(k,1))+(((fricfact2(k,1))*(Uo2(k,1)^2))./s)-
((gravity2(k,1))./s)).*((A.*((exp(root1.*x2))-(exp(root1.*x1))))+(B.*((exp(root2.*x2))-
(exp(root2.*x1)))));
pperc2=(((Uo2(k,1)^2)./s).*((A.*(root1).*((exp(root1.*x2))-
(exp(root1.*x1))))+(B.*(root2).*((exp(root2.*x2))-(exp(root2.*x1))))));

  end
   ppertotch2=ppertotch2+ppera2+pperb2+pperc2;
end
                                                                    % Upadhye (2005)
ppertotch2;%presurre perturbation at otlet or exit of the channel-1
gpertot=gper1in+gper2in  %checking the perturbation of  total mass flow rate
chara=((ppertotch1./gper1in)+(ppertotch2./gper2in));% Characteristic Equation
Rl=real(chara);
Rl1=Rl';
IM=imag(chara);
IM1=IM';

xlswrite('C:\Documents and Settings\umshah2\Desktop\350-50-3-3(3).xls',Rl1);
```

```
xlswrite('C:\Documents and Settings\umshah2\Desktop\350-50-3-3(4).xls',IM1);


plot(chara);



% If Code runs without any trouble till this point that means code ran properly.
fprintf('Code run correctly and terminated properly\n');
```

A.2 PROCEDURE TO RUN THE CODE

Procedure to run the code successfully:

Step 1: Run the SPORTS code:

- For a particular case, set inlet temperature, power, upstream &downstream K factors & guessed stability mass flow rate in SPORTS input file & then run the code. In SPORTS output file properties like Density, velocity, pressure, pressure drop, enthalpy, temperature, C_k, d(rho)/dh are received for each node.

Step 2: Preparation of excel file from the SPORTS output for both the channels:

- Sports output data are imported in excel file through notepad files. This Excel file becomes the input file for linear code.

Step 3: Give meaningful name to the files:

- As there is many trials need to be run for each case, name the excel file in this sequence: value of temperature- power-K factor at the inlet-K factor at the outlet-channel number-mass flow rate. For example a case,

  300-50-0-0-0.085(1).xls

  means case temperature 300 $^{\circ}$C

  power 50KW

  K1=0

  K2=0

  m=0.085kg/s

(1)-Channel 1

Step 4: Create two blank excel files:

- To have an option of final plot in excel also: two blank excel file named the same way except (3) and (4) in the end instead of (1) and (2) for that case.

Step 5: Write the input excel file name with the path on the right side of *xlsread* command in linear code.

Step 6: Write the blank excel file name with the path on the right side of *xlswrite* command of linear code.

Step 7: Set the approximate frequency range in the linear code. e.g. 0 to 2.5

Step 8: Set the actual linear code folder in current directory window of the MATLAB by browsing folder option .

Step 9: There are two options to run the code

(1) Write the file name in command window of MATLAB and press enter.

(2) Right click on the linear code file in current directory window and then choose run command.

Step 10: Receive the characteristics plot in MATLAB file automatically. Another option is to receive the output data in Excel files (3) & (4) and plot the graph manually.

Step 11: Check the curve position in the plane & if not passing from the origin repeat the procedure by changing mass flow rate logically till stability curve received.

Step 12: Save the plots & results.

Step 13: Go for another case & repeat the procedure

APPENDIX -B

B.1 DERIVATION OF LINEARIZED EQUATIONS (Upadhye, 2005)

The non-linear governing equations for this flow system can be summarized as

i. Conservation of Mass (Continuity equation):

$$\frac{\partial \rho}{\partial t} + \frac{\partial (\rho u)}{\partial x} = 0 \tag{4.1}$$

ii. Conservation of Momentum (Momentum transport equation):

$$\frac{\partial (\rho u)}{\partial t} + \frac{\partial (\rho u^2)}{\partial x} + \frac{\partial p}{\partial x} + C_K \rho u^2 + \rho g = 0 \tag{4.2}$$

iii. Conservation of Energy (Energy transport equation):

$$\frac{\partial (\rho h)}{\partial t} + \frac{\partial (\rho u h)}{\partial x} = q_w + \frac{\partial p}{\partial t} \tag{4.3}$$

where, $q_w = \rho \frac{\partial h}{\partial t} + G \frac{\partial h}{\partial x}$ and $\rho = f(h)$ (Chatoorgoon et al., 2005)

Perturbing the conservation of mass equation about the steady state gives

$$\frac{\partial (\rho_0 + \rho')}{\partial t} + \frac{\partial \left[(\rho_0 + \rho')(u_0 + u') \right]}{\partial x} = 0 \tag{b.1}$$

On simplifying Equation (4.b.1) and neglecting the second order terms, gives

$$\frac{\partial \rho'}{\partial t} + \rho_0 \frac{\partial u'}{\partial x} + u' \frac{d\rho_0}{dx} + u_0 \frac{\partial \rho'}{\partial x} + \rho' \frac{du_0}{dx} = 0 \tag{b.2}$$

$$\frac{\partial \rho'}{\partial t} + \frac{\partial G'}{\partial x} = 0 \tag{4.4}$$

Now, similarly perturbing the momentum equation gives

$$\frac{\partial \left[(\rho_0 + \rho')(u_0 + u') \right]}{\partial t} + \frac{\partial \left[(\rho_0 + \rho')(u_0 + u')^2 \right]}{\partial x} + \frac{\partial \left[(p_0 + p') \right]}{\partial x} + C_K \left[(\rho_0 + \rho')(u_0 + u')^2 \right] + (\rho_0 + \rho')g = 0 \tag{b.3}$$

Equation (b.3) can be simplified as

$$\frac{\partial(\rho_0 u')}{\partial t} + \frac{\partial(u_0 \rho')}{\partial t} + \frac{\partial(2u_0\rho_0 u')}{\partial x} + \frac{\partial(u_0^2 \rho')}{\partial x} + \frac{\partial p'}{\partial x} + C_K(2u_0\rho_0 u' + u_0^2\rho') + \rho' g = 0 \tag{b.4}$$

Similarly, perturbing the energy equation about steady state gives

$$\frac{\partial\left[(\rho_0+\rho')(h_0+h')\right]}{\partial t} + \frac{\partial\left[(\rho_0+\rho')(u_0+u')(h_0+h')\right]}{\partial x} = q_w \tag{b.5}$$

While, perturbing energy equation the term $\frac{\partial p}{\partial t}$ is neglected. Simplifying Equation (b.5) yields

$$\rho_0 \frac{\partial h'}{\partial t} + h_0 \frac{\partial \rho'}{\partial t} + h_0 \frac{\partial\left(u_0\rho'\right)}{\partial x} + h_0 \frac{\partial\left(\rho_0 u'\right)}{\partial x} + u_0\rho' \frac{dh_0}{dx} + \rho_0 u' \frac{dh_0}{dx} + u_0\rho_0 \frac{\partial h'}{\partial x} = 0 \tag{b.6}$$

Eliminating the $\frac{\partial \rho'}{\partial t}$ term from the perturbed momentum equation using the perturbed mass equation and using the identities, $\rho_0 u_0 = G_0$, $\frac{dG_0}{dx} = 0$ and the identity given below

$$\rho_0 u_0 \frac{\partial u'}{\partial x} = \frac{\partial\left(\rho_0 u_0 u'\right)}{\partial x} = \rho_0 u' \frac{du_0}{dx} + u_0 u' \frac{d\rho_0}{dx} + \rho_0 u_0 \frac{\partial u'}{\partial x} \tag{b.7}$$

$$\rho_0 \frac{\partial u'}{\partial t} + u_0\rho' \frac{du_0}{dx} + u_0\rho_0 \frac{\partial u'}{\partial x} + \rho_0 u' \frac{du_0}{dx} + C_K(2u_0\rho_0 u' + u_0^2\rho') + \rho' g = -\frac{\partial p'}{\partial x} \tag{b.8}$$

$$\rho_0 \frac{\partial u'}{\partial t} + G_0 \frac{\partial u'}{\partial x} + G' \frac{du_0}{dx} + \frac{\partial p'}{\partial x} + C_K(G_0 u' + u_0 G') + \rho' g = 0 \tag{4.5}$$

This is the final form of the momentum equation that will be used in the further analysis.

Similarly, eliminating $\frac{\partial \rho'}{\partial t}$ from Equation (b.2) using Equation (b.6) gives

$$\rho_0 \frac{\partial h'}{\partial t} + G_0 \frac{\partial h'}{\partial x} + \left(\frac{dh_0}{dx}\right) G' = 0 \qquad (4.6)$$

here $G = \rho u$. (Chatoorgoon et al., 2005)

This is the final form of perturbed energy equation that will be used for further analysis.

Now, perturbing the state equation for the hot as well as the cold side.

Hot-Side:

The state equation on the hot side is given as

$$\rho = \frac{B}{h^{\eta_2}}$$

$$\therefore \ln(\rho) = \ln(B) - \eta_2 \ln(h)$$

Perturbing the above equation about the steady state gives

$$\ln(\rho_0 + \rho') = \ln(B) - \eta_2 \ln(h_0 + h')$$

$$\therefore \ln\left(1 + \frac{\rho'}{\rho_0}\right) = -\eta_2 \ln\left(1 + \frac{h'}{h_0}\right) \qquad (b.9)$$

Expanding using the series expansion of ln(1+x) and neglecting all the second and higher order terms of perturbation, gives

$$\rho' = -\eta_2 \frac{\rho_0 h'}{h_0}$$

Similarly, perturbing the state equation on cold side gives

$$\rho' = \alpha h' \qquad (b.10)$$

Perturbing conservation of mass equation about the steady state and taking the Laplace transform gives,

$$s\tilde{\rho}' + \frac{\partial \tilde{G}'}{\partial x} = 0 \tag{b.11}$$

where, $\tilde{\rho}'$ is Laplace transformed density and $\tilde{G}'$ is Laplace transformed mass flux. For convenience, in further analysis, ρ' will be used for $\tilde{\rho}'$ and G' is used for $\tilde{G}'$. Since $G = \rho u$, the perturbation in mass flux, G' is given as

$$G' = \rho_o u' + u_o \rho' \tag{b.12}$$

Perturbing and taking the Laplace transform of the conservation of energy equation gives,

$$\rho_o s\tilde{h}' + G_o \frac{\partial \tilde{h}'}{\partial x} + \frac{dh_o}{dx}\tilde{G}' = s\tilde{p}' \tag{b.13}$$

For convenience, h' will be used to represent $\tilde{h}'$ in the equations that follow. Expressing ρ' as a function of h' only yields

$$\rho' = \left(\frac{\partial \rho}{\partial h}\right)_p h' \tag{b.14}$$

Substituting Equation (b.14) in Equation (b.11) yields

$$s\left[\left(\frac{\partial \rho}{\partial h}\right)_p h'\right] + \frac{\partial G'}{\partial x} = 0 \tag{b.15}$$

Expressing h' as a function of $\frac{\partial G'}{\partial x}$ using Equation (b.15) yields

$$h' = -\frac{\left(\frac{\partial G'}{\partial x}\right)}{s\left(\frac{\partial \rho}{\partial h}\right)_p} \tag{b.16}$$

Eliminating h' from Equation (b.13) using Equation (b.16) gives

$$s\rho_o\left(-\frac{\left(\frac{\partial G'}{\partial x}\right)}{s\left(\frac{\partial \rho}{\partial h}\right)_p}\right)+G_o\frac{\partial}{\partial x}\left[-\frac{\left(\frac{\partial G'}{\partial x}\right)}{s\left(\frac{\partial \rho}{\partial h}\right)_p}\right]+\frac{dh_o}{dx}G'=sp' \qquad (b.17)$$

Equation (b.17) can be further simplified as

$$\left[\frac{\rho_o}{\left(\frac{\partial \rho}{\partial h}\right)_p}\right]\frac{\partial G'}{\partial x}+G_o\left(\left(\frac{\left(\frac{\partial^2 G'}{\partial x^2}\right)}{s\left(\frac{\partial \rho}{\partial h}\right)_p}-\left(\frac{\partial G'}{\partial x}\right)\frac{\partial}{\partial x}\left[\frac{1}{s\left(\frac{\partial \rho}{\partial h}\right)_p}\right]\right)\right)+\frac{dh_o}{dx}G'=sp' \qquad (b.18)$$

Rearranging the terms of Equation (b.18) gives

$$\left(-\frac{G_o}{s\left(\frac{\partial \rho}{\partial h}\right)_p}\right)\left(\frac{\partial^2 G'}{\partial x^2}\right)+\left[\left(-\frac{\rho_o}{\left(\frac{\partial \rho}{\partial h}\right)_p}\right)-G_o\frac{\partial}{\partial x}\left(\frac{1}{s\left(\frac{\partial \rho}{\partial h}\right)_p}\right)\right]\frac{\partial G'}{\partial x}+\frac{dh_o}{dx}G'=sp' \qquad (b.19)$$

Dividing both sides of Equation (b.19) by $-\frac{G_o}{s\left(\frac{\partial \rho}{\partial h}\right)_p}$ yields

$$\left(\frac{\partial^2 G'}{\partial x^2}\right)+\left[\frac{s}{u_o}+\left(\frac{\partial \rho}{\partial h}\right)_p\frac{\partial}{\partial x}\left(\frac{1}{\left(\frac{\partial \rho}{\partial h}\right)_p}\right)\right]\frac{\partial G'}{\partial x}+\left[\frac{s}{G_o}\left(\frac{\partial \rho}{\partial h}\right)_p\left(\frac{dh_o}{dx}\right)\right]G'=\left[\frac{s^2}{G_o}\left(\frac{\partial \rho}{\partial h}\right)_p\right]p' \qquad (b.20)$$

The above equation is the combined mass and energy equation. Perturbing the momentum equation and taking the Laplace transform gives

$$s\tilde{G}'+G_o\frac{\partial \tilde{u}'}{\partial x}+\tilde{u}'\frac{dG_o}{dx}+\tilde{G}'\frac{du_o}{dx}+u_o\frac{\partial \tilde{G}'}{\partial x}+\frac{\partial \tilde{p}'}{\partial x}+C_K(G_o\tilde{u}'+u_o\tilde{G}')+g\tilde{\rho}'=0$$

(b.21)

For convenience G', u', p' and ρ' will be used to represent $\tilde{G}'$, $\tilde{u}'$, $\tilde{p}'$ and $\tilde{\rho}'$ respectively.

Noting that $\frac{dG_o}{dx} = 0$, Equation (b.21) becomes

$$sG' + G_o\frac{\partial u'}{\partial x} + G'\frac{du_o}{dx} + u_o\frac{\partial G'}{\partial x} + \frac{\partial p'}{\partial x} + C_K(G_o u' + u_o G') + g\rho' = 0 \qquad \text{(b.22)}$$

Equation (b.12) can be expressed as $\rho' = \frac{(G' - \rho_o u')}{u_o}$. Substituting for ρ' in Equation (b.11) gives

$$s\left(\frac{(G' - \rho_o u')}{u_o}\right) + \frac{\partial G'}{\partial x} = 0 \qquad \text{(b.23)}$$

On simplifying and using the identity, $G_o \equiv \rho_o u_o$, Equation (b.23) can be expressed as

$$\frac{\partial G'}{\partial x} + \left(\frac{s}{u_o}\right)G' = \left(\frac{sG_o}{u_o^{\,2}}\right)u' \qquad \text{(b.24)}$$

Multiplying both sides by $\frac{u_o^{\,2}}{s}$, yields

$$G_o u' = \left(\frac{u_o^{\,2}}{s}\right)\frac{\partial G'}{\partial x} + u_o G' \qquad \text{(b.25)}$$

Differentiating Equation (b.25) w.r.t. x gives

$$G_o\frac{\partial u'}{\partial x} + u'\frac{dG_o}{dx} = \left(\frac{u_o^{\,2}}{s}\right)\frac{\partial^2 G'}{\partial x^2} + \frac{1}{s}\frac{\partial G'}{\partial x}\frac{d(u_o^{\,2})}{dx} + u_o\frac{\partial G'}{\partial x} + G'\frac{du_o}{dx} \qquad \text{(b.26)}$$

Noting that $\frac{dG_o}{dx} = 0$, Equation (b.26) becomes

$$G_o \frac{\partial u'}{\partial x} = \left(\frac{u_o^2}{s}\right)\frac{\partial^2 G'}{\partial x^2} + \left(\frac{1}{s}\frac{d(u_o^2)}{dx} + u_o\right)\frac{\partial G'}{\partial x} + G'\frac{du_o}{dx} \qquad \text{(b.27)}$$

And from Equation (b.11) ρ' can be expressed as

$$\rho' = \left(\frac{-1}{s}\right)\frac{\partial G'}{\partial x} \qquad \text{(b.28)}$$

Substituting Equation (b.25), Equation (b.27) and Equation (b.28) into Equation (b.22) gives

$$sG' + \left\{\left(\frac{u_o^2}{s}\right)\frac{\partial^2 G'}{\partial x^2} + \left(\frac{1}{s}\frac{d(u_o^2)}{dx} + u_o\right)\frac{\partial G'}{\partial x} + G'\frac{du_o}{dx}\right\} + G'\frac{du_o}{dx} + u_o\frac{\partial G'}{\partial x}$$
$$+ C_K\left(\left(\frac{u_o^2}{s}\right)\frac{\partial G'}{\partial x} + u_o G' + u_o G'\right) + g\left(\frac{-1}{s}\right)\frac{\partial G'}{\partial x} = -\frac{\partial p'}{\partial x} \qquad \text{(b.29)}$$

Equation (b.29) can be simplified to give

$$\left(\frac{u_o^2}{s}\right)\frac{\partial^2 G'}{\partial x^2} + \left[\frac{1}{s}\frac{d(u_o^2)}{dx} + 2u_o + C_K\left(\frac{u_o^2}{s}\right) - \frac{g}{s}\right]\frac{\partial G'}{\partial x} + \left[s + 2\frac{du_o}{dx} + 2C_K u_o\right]G' = -\frac{\partial p'}{\partial x} \qquad \text{(b.30)}$$

Equations b.20 and b.30 form two simultaneous differential equations that can be solved for G'. First, Equation (b.20) is solved completely to obtain the values of $G', \frac{\partial G'}{\partial x}, \frac{\partial^2 G'}{\partial x^2}$ and then Equation (b.30) is integrated to obtain the pressure drop perturbation for a section. The total pressure drop perturbation along the whole loop is given as the sum of the all pressure drop perturbation in each section of the loop.

Equation (b.20) can be written as

$$\left(\frac{\partial^2 G'}{\partial x^2}\right) + \lambda_1\frac{\partial G'}{\partial x} + \lambda_2 G' = C_2 \qquad \text{(b.31)}$$

For all non-heated sections $\left(\frac{dh_o}{dx}\right) = 0$ which implies

$$\left(\frac{\partial^2 G'}{\partial x^2}\right) + \lambda_1 \frac{\partial G'}{\partial x} = C_2 \tag{b.32}$$

The solution of Equation (b.32) is given as

$$G' = A_2 + B_2 e^{-\lambda_1 x} + \frac{C_2}{\lambda_1} x \tag{b.33}$$

Therefore, $\frac{\partial G'}{\partial x}$ and $\frac{\partial^2 G'}{\partial x^2}$ are given as

$$\frac{\partial G'}{\partial x} = -\lambda_1 B_2 e^{-\lambda_1 x} + \frac{C_2}{\lambda_1} \tag{b.34}$$

And

$$\frac{\partial^2 G'}{\partial x^2} = \lambda_1^2 B_2 e^{-\lambda_1 x} \tag{b.35}$$

Constants A_2 and B_2 can be obtained by matching the BC's from the previous section. Solving Equation (b.33) and Equation (b.34) for A_2 and B_2 gives

$$A_2 = G' - \frac{C_2}{\lambda_1} x + \frac{\left(\frac{\partial G'}{\partial x} - \frac{C_2}{\lambda_1}\right)}{\lambda_1} \tag{b.36}$$

$$B_2 = \frac{\left(\frac{\partial G'}{\partial x} - \frac{C_2}{\lambda_1}\right)}{-\lambda_1 e^{-\lambda_1 x}} \tag{b.37}$$

The pressure drop perturbations for the non-heated section between the two points say $x = x_1 = 0$ and $x = x_2$ is given by integrating Equation(b.30) as follows

$$\int_0^{x_2} -\frac{\partial p'}{\partial x}\delta x = \left(\frac{u_o^{\,2}}{s}\right)\int_0^{x_2}\frac{\partial^2 G'}{\partial x^2}\delta x + \left[\frac{1}{s}\frac{d(u_o^{\,2})}{dx} + 2u_o + C_K\left(\frac{u_o^{\,2}}{s}\right) - \frac{g}{s}\right]\int_0^{x_2}\frac{\partial G'}{\partial x}\delta x$$
$$\left[s + 2\frac{du_o}{dx} + 2C_K u_o\right]\int_0^{x_2} G'\delta x$$

(b.38)

Substituting Equation (b.33), Equation (b.34) and Equation (b.35) in Equation (b.38) gives

$$\Delta p_i' = p'(x_1) - p'(x_2) = \left(\frac{u_o^{\,2}}{s}\right)\left[-\lambda_1 B_2(e^{-\lambda_1 x_2} - 1)\right]$$
$$+\left[\frac{1}{s}\frac{d(u_o^{\,2})}{dx} + 2u_o + C_K\left(\frac{u_o^{\,2}}{s}\right) - \frac{g}{s}\right]\left\{B_2(e^{-\lambda_1 x_2} - 1) + \frac{C_2}{\lambda_1}(x_2)\right\}$$
$$+\left[s + 2\frac{du_o}{dx} + 2C_K u_o\right]\left\{A_2(x_2) + \frac{B_2(e^{-\lambda_1 x_2} - 1)}{(-\lambda_1)} + \frac{C_2}{\lambda_1}(x_2^2)\right\}$$

(b.39)

For all heated sections, solution of Equation (b.20) is

$$G' = A_2 e^{\omega_A x} + B_2 e^{\omega_B x} + \frac{C_2}{\lambda_2} \tag{b.40}$$

where, ω_A and ω_B are the roots of the quadratic equation $m^2 + \lambda_1 m + \lambda_2 = 0$ given as

$$\omega_A, \omega_B = \frac{-\lambda_1 \pm \sqrt{\lambda_1^2 - 4\lambda_2}}{2} \tag{b.41}$$

Therefore, $\frac{\partial G'}{\partial x}$ and $\frac{\partial^2 G'}{\partial x^2}$ are

$$\frac{\partial G'}{\partial x} = A_2\omega_A e^{\omega_A x} + B_2\omega_B e^{\omega_B x} \tag{b.42}$$

And

$$\frac{\partial^2 G'}{\partial x^2} = A_2 \omega_A^2 e^{\omega_A x} + B_2 \omega_B^2 e^{\omega_B x} \tag{b.43}$$

Similar to non-heated section, A_2 and B_2 are found from Equation (b.40) and (b.42) by matching the boundary conditions from previous sections. Therefore A_2 and B_2 are given as

$$A_2 = \frac{\left(\omega_B G' - \frac{\partial G'}{\partial x} - \frac{C_2}{\lambda_2}\omega_B\right)}{(\omega_B - \omega_A)e^{\omega_A x}} \tag{b.44}$$

$$B_2 = \frac{\left(\omega_A G' - \frac{\partial G'}{\partial x} - \frac{C_2}{\lambda_2}\omega_A\right)}{(\omega_A - \omega_B)e^{\omega_B x}} \tag{b.45}$$

The pressure drop perturbation for the heated section between the two points say $x = x_1 = 0$ and $x = x_2$ is given by integrating Equation (b.30) as follows

$$\int_0^{x_2} -\frac{\partial p'}{\partial x}\delta x = \left(\frac{u_o^2}{s}\right)\int_0^{x_2}\frac{\partial^2 G'}{\partial x^2}\delta x + \left[\frac{1}{s}\frac{d(u_o^2)}{dx} + 2u_o + C_K\left(\frac{u_o^2}{s}\right) - \frac{g}{s}\right]\int_0^{x_2}\frac{\partial G'}{\partial x}\delta x$$
$$\left[s + 2\frac{du_o}{dx} + 2C_K u_o\right]\int_0^{x_2} G'\delta x \tag{b.46}$$

Using Equation (b.40), Equation (b.42), Equation (b.43) in Equation (b.46) gives

$$\Delta p_i' = p'(x_1) - p'(x_2) = \left(\frac{u_o^2}{s}\right)\left[A_2\omega_A\left(e^{\omega_A x_2} - 1\right) + B_2\omega_B\left(e^{\omega_B x_2} - 1\right)\right]$$
$$+\left[\frac{1}{s}\frac{d(u_o^2)}{dx} + 2u_o + C_K\left(\frac{u_o^2}{s}\right) - \frac{g}{s}\right]\left[A_2\left(e^{\omega_A x_2} - 1\right) + B_2\left(e^{\omega_B x_2} - 1\right)\right]$$
$$+\left[s + 2\frac{du_o}{dx} + 2C_K u_o\right]\left[\frac{A_2\left(e^{\omega_A x_2} - 1\right)}{\omega_A} + \frac{B_2\left(e^{\omega_B x_2} - 1\right)}{\omega_B} + \frac{C_2}{\lambda_2}(x_2)\right] \tag{b.47}$$

Final form of linearized equations, which was used for prediction of stability boundary:

$$p'_{out} = p'_{in} + s(\nu_1 - \frac{\nu_3}{\gamma_2})(\rho'_{out} - \rho'_{in}) + (\nu_3(\frac{\gamma_1}{\gamma_2}) - \nu_2)(G'_{out} - G'_{in}) \tag{4.7}$$

where,

$$\rho'_{out} = -\frac{1}{s}(\frac{\partial G'}{\partial x})_{out} = -\frac{1}{s}(A_1\omega_A e^{\omega_A x_s} + B_1\omega_B e^{\omega_B x_s})$$

$$G'_{out} = -\frac{1}{\gamma_2}(A_1\omega_A e^{\omega_A x_s}(\omega_A + \gamma_1) + B_1\omega_B e^{\omega_B x_s}(\omega_B + \gamma_1))$$

$$\rho_h = (\frac{d\rho}{dh})_p$$

$$A_1 = \frac{(\omega_B G'_{in} + s\rho'_{in})}{(\omega_B - \omega_A)}$$

$$B_1 = \frac{(\omega_B G'_{in} + s\rho'_{in})}{(\omega_A - \omega_B)}$$

$$\omega_A, \omega_B = \frac{-\gamma_1 \pm \sqrt{\gamma_1^2 - 4\gamma_2}}{2}$$

$$\gamma_1 = [\frac{s}{u_0} - \frac{d(\ln \rho_h)}{dx}]$$

$$\gamma_2 = \frac{-s\rho_h}{G_0}(\frac{dh_0}{dx})$$

$$\nu_1 = (\frac{u_0^2}{s})$$

$$\nu_2 = [\frac{1}{s}\frac{d(u_0^2)}{dx} + 2u_0 + C_K(\frac{u_0^2}{s}) - \frac{g}{s}]$$

$$\nu_3 = [s + 2\frac{du_0}{dx} + 2C_K u_0]$$

In the non-heated sections $\frac{dh_0}{dx} = 0$. (Upadhye, 2005)